ABSTRACT

LIN, LINYU. Assessment of the Smoothed Particle Hydrodynamics Method for Nuclear Thermal-Hydraulic Applications. (Under the direction of Dr. Nam T. Dinh).

Smoothed Particle Hydrodynamics (SPH) is a particle-based Computational Fluid Dynamics (CFD) method that has gained popularity in the last decade in simulation and visualization of fluid flow phenomena and processes. As an advantage over Eulerian techniques, the SPH based on Lagrangian method does not require a numerical gird. Therefore, SPH avoids Eulerian treatment of phasic interface as in Volume of Fluid or Level Set methods. The SPH method has been applied for fluid flow simulation over a broad range of length scale, from ocean tsunami to capillary flow. The present study is focused on evaluation the SPH-based capability for numerical simulation of thermal-hydraulics processes of importance for design and safety analysis of nuclear power plants.

The present study assesses the SPH capability in three areas: hydrodynamics, interface dynamics, and surface effects. The capability for simulation of internal and external free surface flow is evaluated using a suite of numerical benchmarks. The simulation results are compared with experiments and/or results of high-fidelity mesh-based CFD simulations. Micro-SPH, a computer code based on SPHysics package, is developed with built-in surface tension and wettability models. A number of tests for micro-flow are also performed. The benchmarks exhibit a reasonable agreement that demonstrates the capability of SPH method in capturing both micro- (micro-meter) and macro-scale (from fraction of a meter and larger) hydrodynamics.

Assessment of the Smoothed Particle Hydrodynamics method for Nuclear Thermal-Hydraulic Applications

by
Linyu Lin

A thesis submitted to the Graduate Faculty of
North Carolina State University
in partial fulfillment of the
requirements for the degree of
Master of Science

Nuclear Engineering

Raleigh, North Carolina

2016

APPROVED BY:

_____	_____
Dr. Nam T. Dinh Committee Chair	Dr. Igor A. Bolotnov
_____	
Dr. Maria N. Avramova	

DEDICATION

To my parents

BIOGRAPHY

The Author graduated from University of Michigan, Ann Arbor with a bachelor degree in Nuclear Engineering in 2013. He joined NCSU nuclear engineering department in 2014 and passed his PhD qualifying exam in 2015. He started to work with Dr. Nam T. Dinh from 2014. The author expects to continue his research after completing his master degree.

ACKNOWLEDGMENTS

I would like to appreciate Dr. Nam T. Dinh for guiding my research. He has given me lots of suggestions and helps when I write my thesis. I also appreciate the insightful comments from Dr. Igor A. Bolotnov and Dr. Maria Avramova on the content of this work. I like to thank researchers at Idaho National Laboratory Dr. Curtis Smith and Mr. Steven Prescott, and Centroid Pic researchers Ram Sampat, and Dr. Nadir Akinci, and Dr. Anh Bui for their support in various stages of this work. The support by the U.S. Department of Energy through the Consortium for Advanced Simulation of Light Water Reactors (CASL) and the Idaho National Laboratory's National University Consortium program is gratefully acknowledged.

TABLE OF CONTENTS

LIST OF TABLES

LIST OF FIGURES

1. Introduction

For a long time, it is believed that the behavior of the near-wall liquid layer plays a key role in boiling heat transfer and boiling crisis [1] [2] [3]. The surface properties are found to play an important role in enhancing or reducing the Critical Heat Flux (CHF). A large body of experimental works has been performed to characterize the effect of heater surface roughness, porosity, wettability on critical heat flux [4] [5] [6] [7] [8] [9] [10] [11]. Though physical mechanisms remain unknown, researchers have developed a basic understanding about the effect of surface characteristics on CHF. For example, the hydrophilic smooth surfaces tend to have larger CHF than hydrophobic surfaces; surface porosity tends to enhance the CHF, especially when it's coupled with high wettability. However, discrepancies still exist because the experiments for studying surface phenomena are hard to set up and measured. Several computational models [12] [13], like one based on the lubrication theory [14], are used to explain the mechanism. However, such models are currently limited to one-dimensional formulation and unable to deal with the dry-out phenomena. In this case, methods of Computational Fluid Dynamics (CFD) have potential for the mechanistic study of boiling.

Since the invention of CFD, many methods are proposed and developed. Taking advantage of computer power, different techniques are used to solve Navier-Stokes Equations, many of which are able to effectively explain and predict flow pattern in aerospace and mechanical engineering. Mesh-based methods, as one of the Eulerian methods, have become one of the most successful CFD tools for fluid simulation. The two-fluid model is proposed for multiphase problem [15] [16]. Assuming continuum and thermodynamic equilibrium the two sets of Navier-Stokes Equations are averaged over suitable control volumes and time scale across the interface. Closure laws are included to provide correlations and parameters for interface properties, including viscous stress tensor, viscosities, pressures and drag. These parameters such as drag coefficients [15] [17], transient forces [15] [18] and interfacial area [15] [19] are usually measured by experiments. However, it becomes more difficult for problems with smaller scales and more phenomena, when closure laws and parameters are hard to define. On the other hand, some DNS models such as level-set [20] [21] and volume of fluid (VoF) methods [22] [23] are developed for multiphase simulation using very fine mesh. Though level set method can track the interface easily on unstructured grids, it is infamous for the mass loss problem.

Lagrangian methods, as another major branch of numerical methods in CFD, discretize the space with moving particles and solve systems of discrete equations by calculating the interactions between particles. As the Eulerian methods have some problems dealing with interfaces or simulating flow over complex boundary with large gradient, Lagrangian methods work much better on these types of scenarios. Many Lagrangian numerical algorithms such as Dissipative Particle Dynamics (DPD) and Smoothed Particles Hydrodynamics (SPH) are developed to simulate fluid dynamics in both macro and micro scales. Though the particle methods are usually more computationally expensive than Eulerian methods, it's much easier to deal with interfacial problem with particles. With growing computing power and decreasing expense of data computation and storage the Lagrangian methods gain a lot of attentions in fluid simulation. Computer codes such as SPHysics [24] and LAMMPS-SPH [25] have been developed for fluid dynamics simulations in both macro and micro scales. SPH is especially good at dealing with shock wave problem [26] [27] [28], and recently several applications of SPH in flooding

simulations are presented in [29] [30] [31]. However, the particle approximation in SPH may also cause some numerical problems such as particle inconsistency and tensile instability [32]. Also efficiency is another problem for SPH methods, because SPH needs a large number of to ensure the accuracy and adaptive particle size is hard to achieve. This study attempts to assess a CFD tool for use in nuclear thermal-hydraulic applications including flooding and micro-hydrodynamics.

1.1. Scenarios, Processes and Phenomena of Interest

1.1.1. Micro-hydrodynamics in Boiling

1.1.1.1. Overview

Performance of boiling equipment is limited by a transition from "nucleate" to "film" boiling. This transition region is known as "burn out" and it's characterized by a dried out heater surface and accompanied by the ultimate physical destruction of the heater. The phenomenon that causes this transition is called boiling crisis and the heat flux at which this burn out occurs is called critical heat flux (CHF). Fundamental to the physics of boiling crisis is evaporating liquid layer adjacent to the heater surface. The existence of thin liquid film, also referred as micro-layers, has been confirmed experimentally by Sharp [33] and Jawurek [34]. The liquid layer is attached to the heater surface, beneath vapor bubbles. Though the thickness of the layer is only few micrometers, the heat flux through the layer can exceed $1MW/m^2$ [35]. It's proposed by Theofanous et al. [2] that the hydrodynamics action of the micrometer-scale liquid layers defines the mechanism that leads to "burn out". Figure 1 shows the structure of the burn-out investigation, which turns out to be a multi-scale problem. For this type of problem, interactions of micro-layer with macro-hydrodynamic and surface will control the boiling process. This model explains well the effects of forced flow and surface features on CHF. However, the film is so thin that direct measurement is hard to accomplish.

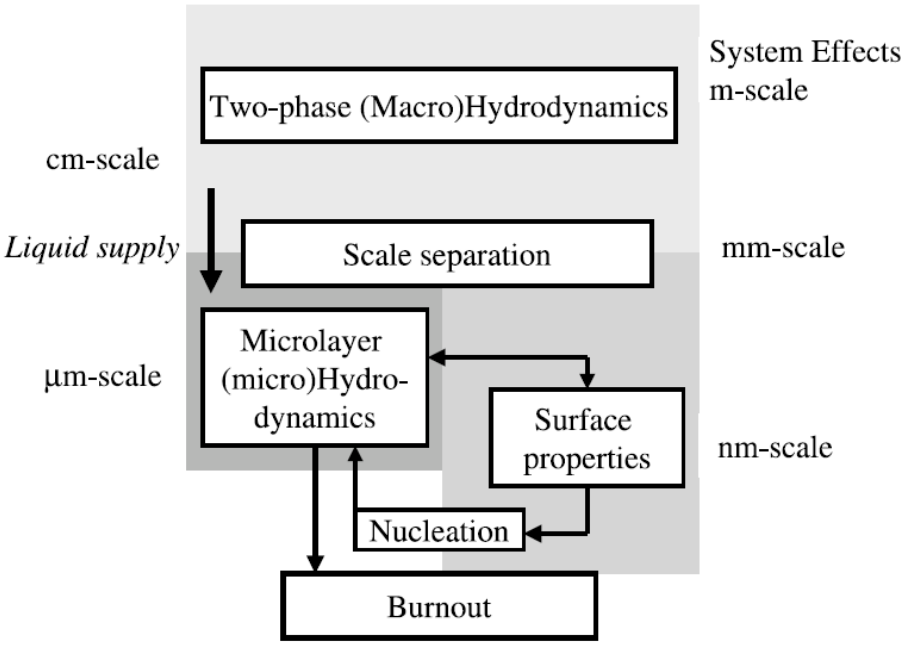

Figure 1: Schematic of scale separation process in boiling and its relations to burnout from Theofanous et al, 2002 **[2]**

By looking at the simulation of vapor bubble nucleation progress made by Dinh et al. [1] shown in Figure 2, it can be seen that after the bubble collapses, a dry spot was left behind and liquid film tried to get back and rewet this spot. In other word, the rewetting ability of the returning liquid film directly prevents the occurrence of dry spot. If the dry spot exists for long enough time, heater surface burn-out will happens. So it becomes necessary to look carefully into the returning liquid film mechanism and features that affect its rewetting ability.

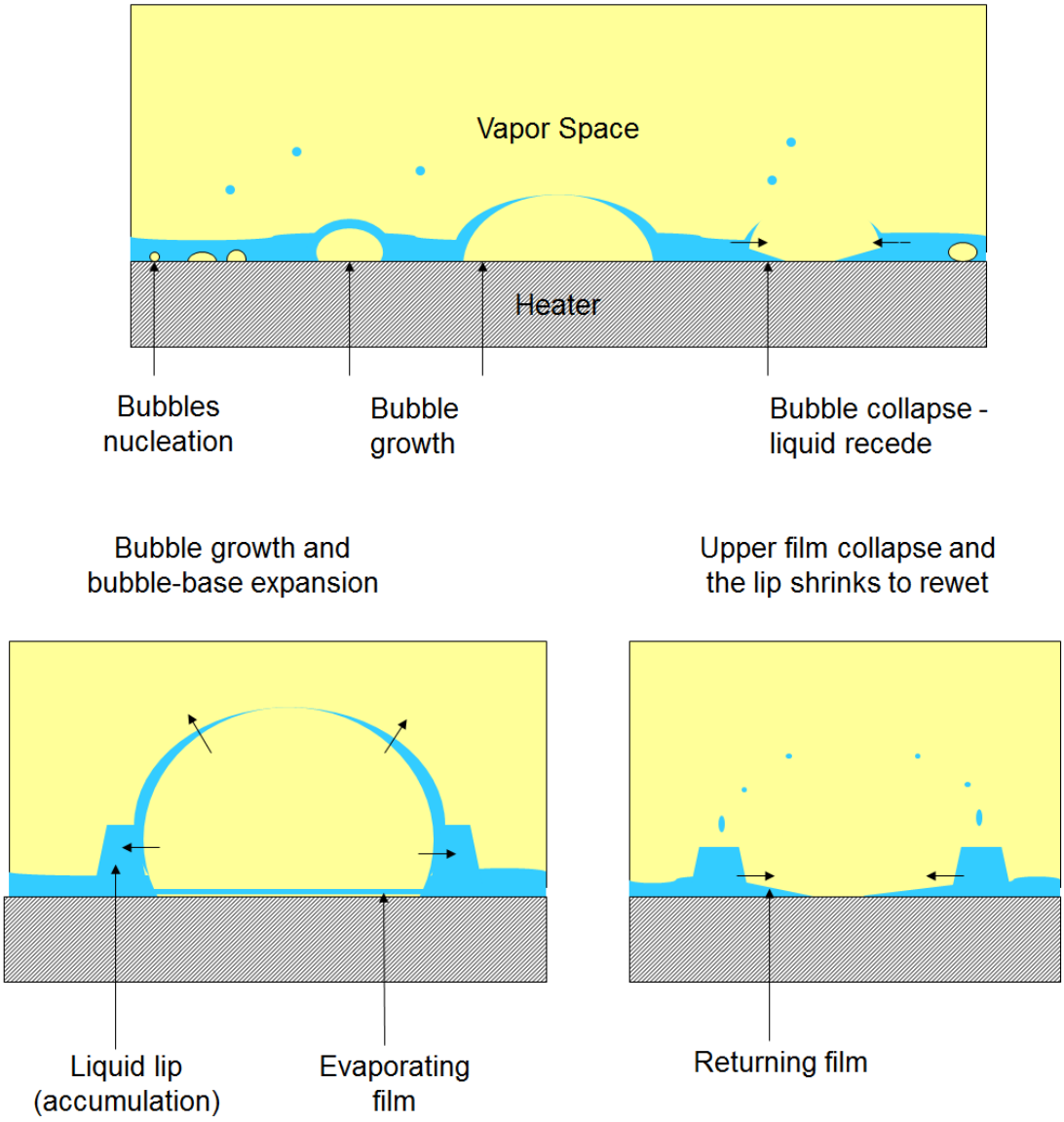

Figure 2: Conceptual plots of vapor bubble nucleation and bursting process in a liquid film from Dinh et al 2007 **[1]**(top: general progress; bottom: key frame of the bubble dynamics)

1.1.1.2. PIRT and Parameter Domain

First step in studying micro-hydrodynamics of boiling is the key phenomenon identification. The Phenomena Identification and Ranking Table (PIRT) is a ranking table to align application technical requirements with associated physics and materials models, simulation code capabilities and verification, validation and uncertainty quantification activities [36]. It's developed to identify and prioritize important physical phenomena in an application and to assess the adequacy/gaps of the current simulation capabilities. The PIRT helps to ensure both sufficiency and efficiency by expert elicitation and prioritization of the analysis of the simulation and experimental capabilities.

In facts, there are lots of factors that could affect the rewetting ability such as surface characteristics and hydrodynamics of both macro-level and micro-level. (PIRT) is conducted to assess the key phenomena and their corresponding importance and adequacy for micro-hydrodynamics of boiling. The figures of merit are:

(1) Timing of micro-layer rewetting dry surface [1] [2]

(2) Effects of surface features [4] [5] [7] [10] [11].

Based on the figures of merit, the key phenomena in micro-hydrodynamics problem are:

(1) Hydrodynamics

This phenomenon includes a) Flow models such as laminar and turbulence models and b) Flow over structured surface. They are designed to determine the hydrodynamics of micro-layer.

(2) Interface Dynamics

This phenomenon includes a) Interface tracking and b) Capillarity effects. They are designed to capture the tri-contact line of micro-layer.

(3) Energy

This phenomenon includes a) Energy transfer and b) Phase change. They are designed to simulate thermal properties during the boiling. Note this study focuses on isothermal scenario and energy has not yet considered.

(4) Surface Effect

This phenomenon includes a) Textured surface; b) Surface porosity; and c) Surface roughness. They are designed to investigate the effect of surface features. Currently only very simple textured surfaces with single structure are considered. Surface porosity and roughness are not yet included.

Table 1 presents the PIRT table for micro-hydrodynamics of boiling. There are three levels in “Imp” column, representing the “High”, “Median”, and “Low” importance of specific phenomenon. There are three aspects in Adequacy rankings: Mathematical Model, Computational Code and Validation. Similar to Important ranking, three levels exists for every aspect. Note that “High” means there are adequate resources of certain aspect, while “Low” means there are few resources and more studies are needed.

Table 1: Phenomena Identification and Ranking Table of micro-hydrodynamics in boiling

ID	Phenomena	Imp	Adequacy		
			Math Model	Code	Val
A	Energy	M			
	Heat transfer	H	M	M	M
	Phase change	H	M	M	M
B	Hydrodynamics	H			
	Laminar flow	H	H	H	H
	Turbulence flow	L	M	M	M
	Flow over structured surface	H	M	M	M
C	Interface Dynamics	H			
	Interface tracking	H	M	M	L
	Capillarity force (Contact Angle)	H	L	L	L
D	Surface Effect	H			
	Textured Surface	H	L	L	L
	Porosity	H	L	L	L
	Roughness	H	M	M	M

As a result, more attentions should be paid to interface dynamic and surface science, because they have high importance ranking, but with relative low adequacy in both model and validation.

1.1.1.3. Research Question

A large number of experiments were conducted to investigate the effect of heater surface characteristics on boiling heat transfer [6] [7] [9] but no clear quantitative relation has been found. Some experiments even show inconsistent results for the same surface features. Table 2 shows part of experimental results from research paper.

Table 2: Experimental results from available research paper about separate effects of surface features on CHF

Surface Features	Effects on CHF
Wettability	Improve [7] [10] Improve only when combined with porosity [6]
Porosity	Improve (60%) [6]
Roughness	Improve [4] [5] [7] [11] No effect alone [6]
Channel Spacing	Improve till Maximum then degrade [9]
Force Flow	Improve and more for shear-driven flow [8]

Experimental measurements help people understand the phenomena and propose possible interpretations, they can also provide empirical correlations for CHF prediction with satisfactory accuracy. However, when the governing mechanism is complex, experiments alone may not

provide accurate insights and resulting correlations may have high uncertainty, which would increase uncertainty of model predictions. Also, because of the complexity of micro-scale hydrodynamics, where some features may not be independent, so empirical model can be oversampled, which led to additional prediction uncertainty. Figure 3 shows the schematic plot of different technical approaches for investigating surface effect on CHF.

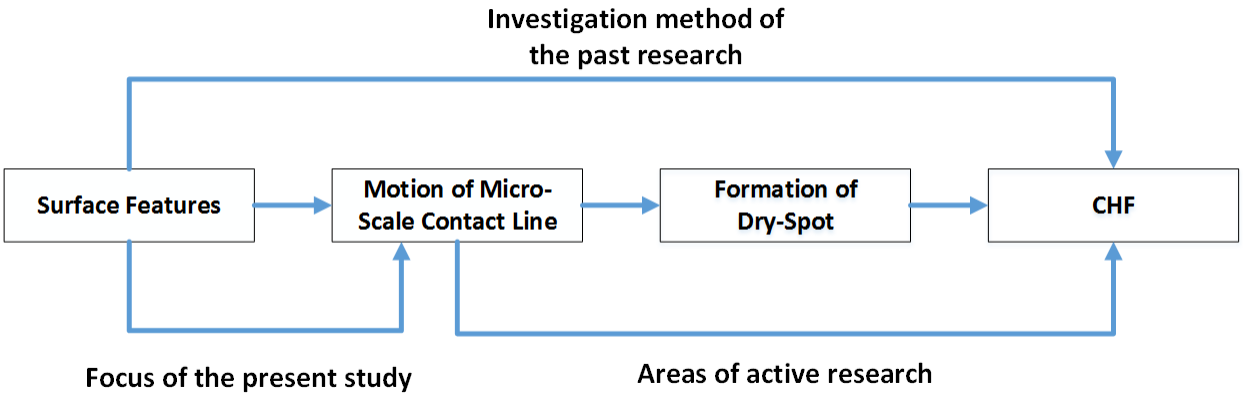

Figure 3: Schematic of currently available research works and the position of the approach used in micro-hydrodynamic study

1.2. Computational Fluid Dynamics Methods

Nowadays, several simulation methods are developed for CFD simulation. The simulation translate physical problem into a discrete form of mathematical description. With increasing computer power, a CFD codes can provide insights and complete information that cannot be directly measured or observed. Currently, there are two major types of numerical CFD methods: Grid-based methods and Mesh-free methods. Conventional grid-based numerical methods such as FDM and FEM have been widely applied to CFD application and have become the dominant methods in numerical simulation. As its name indicates, mesh construction is required for every grid-based methods, which led to additional efforts for building irregular or complex geometry [37] [38]. Also when the precise location of inhomogeneity is needed (e.g., free surface, deformable boundaries, and moving interfaces), it becomes much more difficult and expensive to solve the problem. A recent interest has been brought to mesh-free methods, whose key idea is to build numerical solution for integral equations or PDEs with sets of arbitrarily distributed nodes or particles. Because properties are stored in each artificial particle, mesh-free methods can deal with free surface, moving interface, complex geometries. In addition, it is less challenging to achieve fully parallel algorithms [32] compared to mesh-based methods. With the development of fast and massively parallel computers, particle-based methods are becoming more and more popular. Table 3 shows the required phenomena and code's capability for studying of micro-hydrodynamics in boiling. Among the three different computational methods assessed, the particle-based method is the best-fitted methods for this study. Following work will focus on assessment of SPH in nuclear applications from flooding to micro-hydrodynamics.

Table 3: Phenomena and adequacy of CFD methods for investigation of micro-hydrodynamics in boiling

Phenomena		Eulerian Methods	Particle-based Methods
Hydrodynamics	Laminar flow	H	H
	Turbulence flow	H	M
	Flow over structured surface	M	H
Interface Dynamics	Capillarity	H	H
	Interface tracking	H	H
Energy	Energy transfer	H	M
	Phase change	M	M
Surface Effects	Structured surface	M	H
	Porosity	L	H

1.3. Particle-based Methods: State of the Art

Particle based numerical methods are usually composed of finite number of discrete particles to represent the state of a system and to record the movement of an object. In CFD aspect, each particle possesses a set of field variables (e.g., mass, velocity, position, energy). The particles-based methods has been used in multiple scales, which can be divided as: microscopic, mesoscopic, and macroscopic scale particle methods. A typical example of microscopic particle-based methods is Molecular Dynamics (MD), where the force potential function is used to represent the interaction between particles. For mesoscopic methods, the Dissipative Particle Dynamics (DPD) [39] is widely used for simulating properties of fluids. In DPD methods, particles represent a region of molecules rather than single atoms, which gives access to longer time and length scales than MD simulations. Macroscopic particle-based methods (e.g., SPH proposed by Gingold and Monaghan [40] and Particle-in-Cell) usually divide the fluid into a set of discrete elements. The elements are represented as particles and the properties possessed are distributed and smoothed across a spatial distance (smoothing length) by certain rule (e.g., kernel function). Thus physical quantity of any particle can be obtained by summing the relevant properties of all the particles lying within the range of kernel. In SPH, the summing of property or function f is governed by:

$$f(\vec{r}) = \int f(\vec{r}')W(\vec{r} - \vec{r}', h)d\vec{r}' \quad \text{Eq. 1}$$

where h is the smoothing length and $W(\vec{r}-\vec{r}',h)$ is the kernel function that weigh the properties during summing process. In discrete notation, the equation becomes:

$$f(\vec{r}) = \sum_b f\left(\vec{r}_b \right) W\left(\vec{r} - \overrightarrow{r_b} \ , h\right) \Delta V_b \quad \text{Eq. 2}$$

where b represents any discrete region within the affecting region, if particles approximation is used in each region and the function f, the equation will be will then be written as:

$$< f(\overrightarrow{r_a}) >= \sum_b \frac{m_b}{\rho_b} f\left(\vec{r}_b \right) W\left(\overrightarrow{r_a} - \vec{r}_b \ , h\right) \quad \text{Eq. 3}$$

m_b and ρ_b represents the mass and density of each particle. Note that mass and density are introduced during the particle approximation. This makes SPH very suitable to be applied in hydrodynamics problems where mass and density are very important parameters to determine.

In general, particle-based methods can be applied to a very large scale of problems with fairly high fidelity. Even the microscopic methods mentioned before can be applied from astrophysics to micro-hydrodynamic fluid problems. Notably, the major issue is the balance between accuracy and efficiency.

1.4. Verification and Validation (V&V)

Model verification is often defined as "ensuring that the computer program of the computerized model and its implementation are correct [41]" and the validation is defined as "substantiation that a computerized model within its domain of applicability possesses a satisfactory range of accuracy consistent with intended application of the model [42]". Validation process is usually composed of two parts: accuracy assessment and adequacy assessment (PIRT analysis). Verification is achieved by comparing the simulation results with analytical solution, which is straightforward and accurate. However, due to constrain of applying analytical solution, sometime no analytical solution exists for certain complex problem. Special statistical techniques (e.g., database and Physics-Guided Coverage Mapping) are needed for simulation code V&V. In this work, the V&V is achieved by comparing the numerical solutions of SPH either to analytical solution and fine-mesh numerical output, or directly to experimental measurements.

1.5. Evaluation Model Development and Assessment Process (EMDAP) **[43]**

EMDAP is a systematic process described by NRC to assess the models used in nuclear accident calculations and to estimate and reduce uncertainty of these models. Evaluation model (EM) is the calculation framework for evaluating the behavior of the model and it includes the computer programs, special models and all other information needed to apply the calculation framework to a specific event. Based on the PIRT in section 1.1, the EM in this study includes: (1) SPH-based hydrodynamic model (2) Interface dynamics including surface tension and wettability; (3) Surface. Note that the energy portion is not fulfilled in this study. During this assessment process, some basic principles are identified as important to follow [43]:

1. Determine requirements for the evaluation model

2. Develop an assessment base consistent with the determined requirements

3. Develop the evaluation model
4. Assess the adequacy of the evaluation model

Details and relations between these four elements is shown in Figure 4.

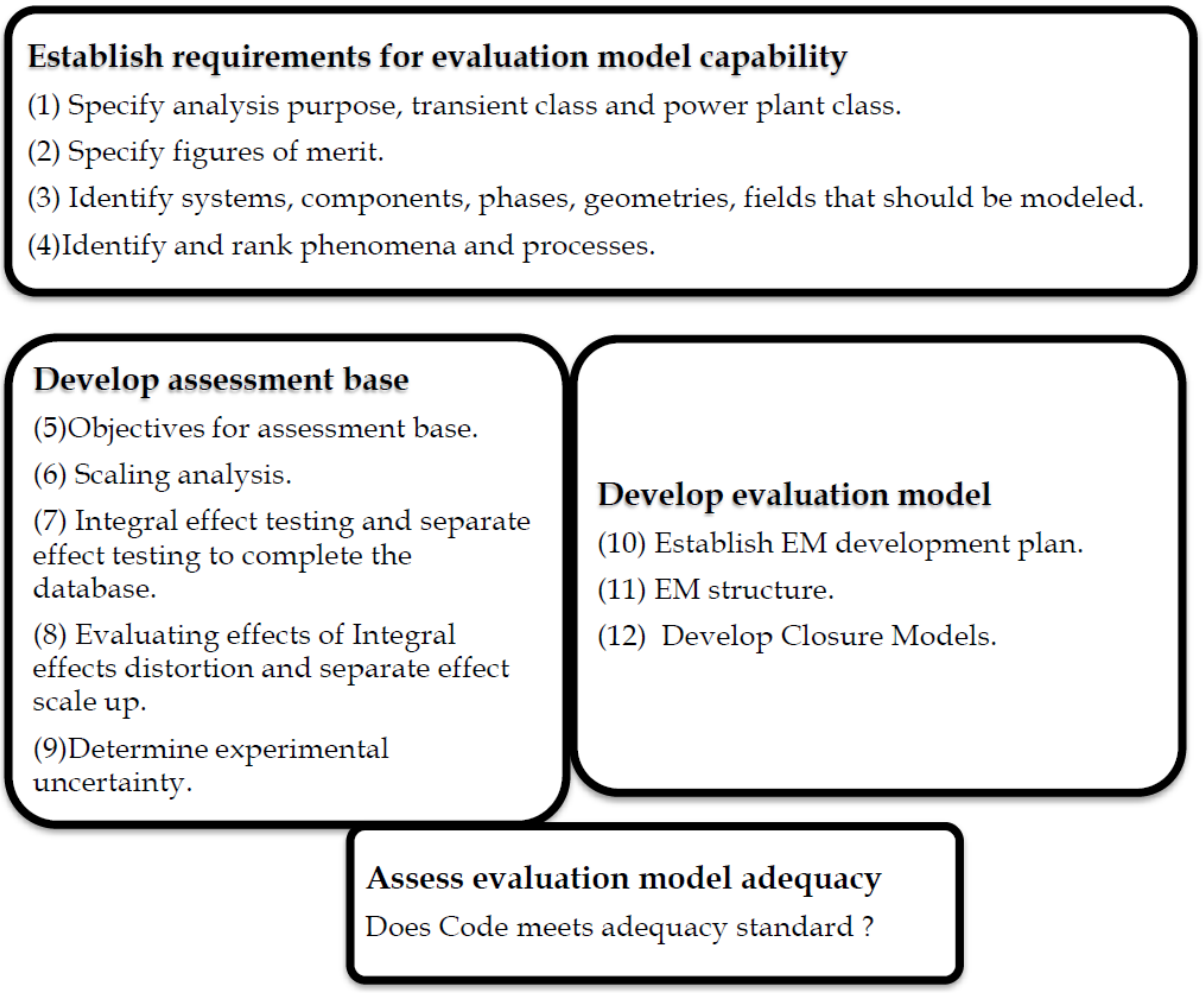

Figure 4: Details and relations of four elements in EMDAP **[43]**

Principle (1) is stated in section 1.1.1 and **Error! Reference source not found.** with analysis purpose, figures of merit and phenomena ranking. The second and third principles are skipped in this study because a set of experiments are needed for the scaling analysis and uncertainties. The last principle is accomplished by running multiple numerical experiments using the EM and assessing its fidelity and/or accuracy by comparing the results to experimental data, analytical solution or numerical data from fine-mesh simulations. The scalability is checked by running convergence study.

1.6. Overview of SPH Codes

There are several SPH-based fluid program available nowadays. Because SPH can produce nice visualizations, it's popular in computer graphic. People has successfully build SPH into GPU, which greatly improve the calculation speed and make it comparable to traditional grid-based methods. Currently, there are three popular SPH software packages: SPHysics [24], LAMMPS-SPH [25] and NEUTRINO [44]. SPHysics and LAMMPS-SPH are open-source and can be found online, Neutrino is designed for commercial usage and it only has beta version for now.

SPHysics is compiled in FORTRAN, while its new version Dual-SPHysics is developed on C++. Currently it can run flooding simulation with several million of particles. LAMMPS is a MD program and because of the similarity between MD and SPH as mentioned in Section 1.3. LAMMPS opens its kernel to user, which is mainly particle setup and searching, boundary conditions and so on, user can call these functions or build their own functions based on the available kernels. Neutrino is another SPH program originally developed by Ram Sampath and Nadir Akinci [45] [46] [47], currently it's used for the external and internal flooding simulation by Idaho National Laboratory. Neutrino has user-friendly interface, user can change parameters directly in the GUI. The simulation results can be visualized without post-processing tools. User can also stop the simulation at any time, change some parameter and continue to run the program. Table 4 shows some major difference between these SPH software packages. Note the computational speeds of three packages are obtained by running dam break simulation with the same geometry.

Table 4: Comparison of three popular SPH software: NEUTRINO, LAMMPS and (Dual-)SPHysics. Dual-SPHysics (written in C++) is the new version of SPHysics (written in FORTRAN)

	Neutrino	LAMMPS	<Dual->SPHysics
Language	C++, OpenGL, Qtcreator	C++	<C++> Fortran
Fluid Solver	IISPH [48]	WCSPH	WCSPH
Solid Solver	Yes	Reported in SMD-LAMMPS [49]	No Additional
Surface tension and Wettability	Simplified CSF [45]	Reported in LAMMPS-SPH-multiphase [50]	No
Turbulence Model	No	No	SPS Turbulence Model
Heat Transfer	No (No Energy Eqn.)	Available	No
Parallel Computing	Yes (shared memory)	Yes (MPI)	<GPU/Parallel>Series
Computational Speed	8.50×10^{-7} $sec/\Delta t \cdot particle$	2.09×10^{-6} $sec/\Delta t \cdot particle$	1.24×10^{-5} $sec/\Delta t \cdot particle$

It can be seen that SPHysics and LAMMPS are friendlier to researchers because they are open-source and have several user packages. Both of them can be run on cluster with multiple computational nodes. While NEUTRINO is based on openMP and has shared memory, it's not able to run on cluster. But its good visualizations and friendly user interface render it capability in

doing certain engineering applications, for example, to analyze the risk of flooding impact onto a nuclear power plant. In this study, SPHysics is employed for the most cases. NEUTRINO serves as a supplementary for cases with particle number larger than 500K.

1.7. Objective and Technical Approaches

After selecting SPH as the CFD tool, the objective of this study becomes to assess the capability of SPH in flooding and micro-hydrodynamics in boiling. The assessment in this study is fulfilled by doing theoretical analysis and systematic evaluation through numerical benchmarks. Note from section 1.6 that most existing SPH programs focus on large scale simulations, so before the assessment of SPH's capability in micro-hydrodynamics, a physical capillarity model including surface tension and wettability is needed for SPH. It can also be seen from PIRT of flooding and boiling that phenomena required by flooding are included in boiling. By doing non-dimensionalization study, the number of assessments that is needed can be greatly reduced. In this study, the capability of SPH in micro-hydrodynamics is mainly evaluated. Figure 5 shows the flow chart of applying Micro-SPH, a new SPH program with capability of investigating micro-hydrodynamics, into the investigation of surface effect on CHF.

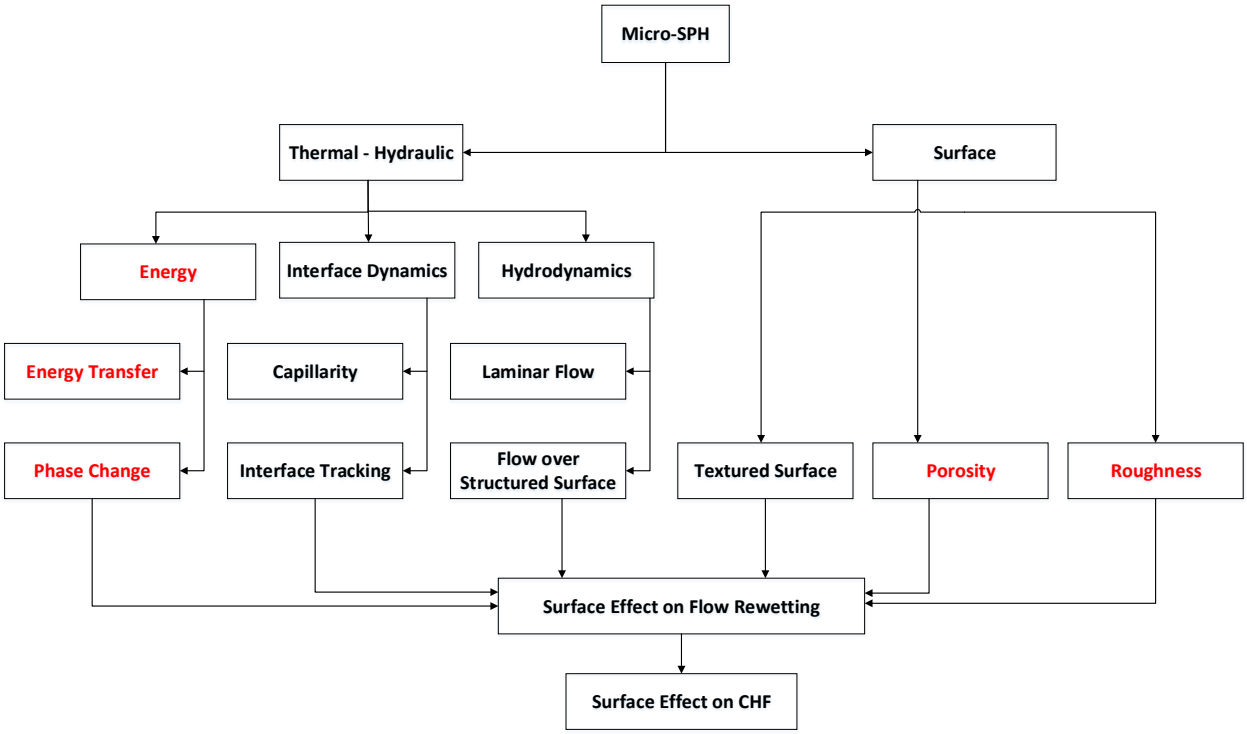

Figure 5: Flow chart of applying Micro-SPH in CHF investigation and the desired features in Micro-SPH

As mentioned, some important features, like heat transfer, phase change and some complex surface structures, are still missing in this study. In fact, how to achieve phase change and non-isothermal condition in SPH still remains to be a challenge. Currently, Micro-SPH is capable of investigating surface effects on isothermal fluid wetting process. Table 5 shows the phenomena and corresponding strategies and test cases employed in SPH. The performances of each test are

evaluated to assess the capability of SPH in each phenomena. Appendix A shows all the subroutines in Micro-SPH. **Appendix B** shows the code structure.

Table 5: List of Phenomena, strategies used and test performed for Micro-SPH.

Phenomena	Capability	Solving Strategy	Test Performed
Hydrodynamics	Laminar flow	Particle discretization of N-S mass and momentum function	Poiseuille flow; Lid-Driven cavity flow;
	Flow over structured surface	Stationary layer(s) of particles sharing properties with fluid	Collapse of water column; Flow around cylinder;
Interface Dynamics	Capillarity	CSF [45] and adhesion model	Droplet Oscillation; Drop contacting surface; Capillary Rise between parallel plates;
	Interface tracking	Color function	Interface reconstruction;
Surface	Textured surface	Stationary layer(s) of particles sharing properties with fluid	Flow around cylinder; 3D dam break;

2. Smoothed Particle Hydrodynamics

2.1. History

Smoothed Particle Hydrodynamics is invented to deal with astrophysical problems in three-dimensional open space [40] [51] where the collective movement of particles is similar to the movement of liquid or gas flow. Early SPH algorithms are derived from the probability theory and statistical mechanics are used for the numerical estimation [27]. With the extensive application of SPH, new algorithm with both linear [40] [52] and angular momentum [53] is developed.

2.2. Standard Formulation

2.2.1. Kernel Function

Smoothing kernel is critical for the performance of SPH simulation. It should decrease monotonically with the increasing of distance, and tends to be delta function as h goes to zero [29] [54] [55]. In this study, two major kernel functions are used in simulation:

Cubic:

$$W(q) = \frac{10}{7\pi h^2}\begin{cases} 1 - \frac{3}{2}q^2 + \frac{3}{4}q^3, & 0 < q \leq 1 \\ \frac{1}{4}(2-q)^3, & 1 < q \leq 2 \\ 0, & 2 < q \end{cases} \quad \text{Eq. 4}$$

Quintic [56]

$$\frac{10}{4\pi h^2}\left(1 - \frac{q}{2}\right)^4 (2q+1), \quad 0 < q < 2 \quad \text{Eq. 5}$$

where q is defined as r/h. The numerical simulation shows that Quintic kernel function can result in more stable results than cubic. However, due to the relative high order (5^{th} order) of Quintic kernel, usually Cubic function is used for efficiency.

2.2.2. Density (Continuity Equation)

There are mainly two approaches to solve the density equation. The traditional method is summation density, which applies SPH approximation to the density directly [54].

$$\rho_a = \sum_b m_b W_{ab} \quad \text{Eq. 6}$$

However, this approach will cause an artificial density decrease near fluid interfaces where not all support regions are covered by particles. Another approach is based on continuity equation and applying SPH approximation to velocity divergence part:

$$\frac{d\rho_a}{dt} = \sum_b m_b \vec{v}_{ab} \vec{\nabla} W_{ab} \quad \text{Eq. 7}$$

Eq. 7 is used in this study, because lots of interface problems will be dealt in current work.

2.2.3. Momentum Equation

2.2.3.1. Pressure

The calculation of pressure term in momentum equation is a major task for any CFD calculation because the gradient of pressure is an important driven force for fluid motion. In SPH incompressible flow can also be achieved by retrain the density to be constant, but it may require extra iteration [48] and cost more computational power. Usually weakly compressible formula, which leads to a concept of artificial compressibility, is applied in most study. As a result, the density will also change slightly. The major idea here is that every theoretically incompressible fluid is actually compressible. There are many types of expression for artificial pressure, in SPHysics, the equation of state proposed by Monaghan [26] is applied:

$$p = B\left(\left(\frac{\rho}{\rho_0}\right)^{\gamma} - 1\right) \qquad \text{Eq. 8}$$

where $\gamma = 7$ is a constant, ρ_0 is the reference density, $B = c_0^2\rho_0/\gamma$ and c_0 is the speed of sound at the reference density.

Noted that the speed of sound is an important parameter to consider, usually the value should be large enough that the behavior of artificial fluid is similar to real fluid. And the value can't be too large, say the real sound speed 1480m/s for water, or artificial compressible can't be achieved. In this study, Morris's [57] [58] conclusion is used to ensure an appropriate selection of sound speed value and the typical sound speed applied in this study is about 10 – 20 m/s:

$$c^2 \sim max\left(\frac{V^2}{\delta}, \frac{\_V}{\delta L}, \frac{FL}{\delta}, \frac{\sigma K}{\rho_0 \delta}\right) \qquad \text{Eq. 9}$$

where each term represents the consideration from speed, viscosity, body force and surface tension respectively, V is the largest value of particle velocity, $\_$ is the kinetic viscosity, F is the magnitude of body force, L is the characteristic length scale, K is the typical curvature.

Then the pressure gradient term of momentum equation can be represented as:

$$\left(\frac{d\vec{v}_a}{dt}\right)_p = -\sum_b m_b \left(\frac{P_b}{\rho_b^2} + \frac{P_a}{\rho_a^2}\right)\vec{\nabla} W_{ab} \qquad \text{Eq. 10}$$

2.2.3.2. Viscosity

There are two types of viscosity models used in this study. First is artificial viscosity proposed by Monaghan [26]. The expression is fairly simple, besides, it effectively prevent unphysical penetration and provides necessary dissipation. Another model is called laminar viscosity developed by Morris [57]. The expression of laminar viscosity is derived from the SPH

approximation of second order derivative. In general, the viscosity term in momentum equation can be represented as:

Artificial Viscosity

$$(\frac{d\vec{v}_a}{dt})_\tau = -\sum_b m_b \prod_{ab} \vec{\nabla} W_{ab} \quad \text{Eq. 11}$$

where

$$\prod_{ab} = \begin{cases} -\frac{\alpha \bar{c}_{ab} h \vec{v}_{ab} \vec{r}_{ab}}{\bar{\rho}_{ab}(\vec{r}^2{}_{ab} + 0.01h^2)}, & \vec{v}_{ab}\vec{r}_{ab} < 0 \\ 0, & \vec{v}_{ab}\vec{r}_{ab} \geq 0 \end{cases} \quad \text{Eq. 12}$$

where α is usually characterized as [59]:

$$\nu = \frac{\alpha h c}{8} \quad \text{Eq. 13}$$

Laminar Viscosity

$$(\frac{d\vec{v}_a}{dt})_\tau = (\nu \nabla^2 \vec{v})_a = \sum_b m_b (\frac{4\nu \vec{r}_{ab} \vec{\nabla} W_{ab}}{(\rho_a + \rho_b |\vec{r}_{ab}|^2)}) \vec{v}_{ab} \quad \text{Eq. 14}$$

2.2.4. Energy

The energy equation is derived by stating that energy change inside a fluid cell should equal to the summation of the net heat flux into the fluid cell and the time rate of work done by the body and surface forces acting on that fluid cell. Then the SPH approximation is applied to the equation and corresponding SPH formula for energy is obtained. Because currently effects due to heat transfer are not the major focus, not too much attention is brought to the energy equation. But this part is so important to the research in micro-hydrodynamics that a careful look into this problem is needed for future work.

2.2.5. Particle Searching

Because the kernel function only applies to a finite support domain, a searching algorithm is needed to find all particles inside the region. Currently there are three popular searching algorithms: all-pair search, linked-list search and tree search algorithm. In SPHysics code, linked-list searching is applied, all particles are assigned to cells as shown and identified through linked list. Starting from the left lower corner, particles inside cell ik will only interact with particles inside adjacent cells of NW, N, NE and E. The other half side of W, S, SW and SE is calculated using reverse interaction. The computational time of linked-list methods save computational time greatly. Compared to all-pair search, it saves the number of calculations per time step from N^2 to $NlogN$, where N is the number of particles.

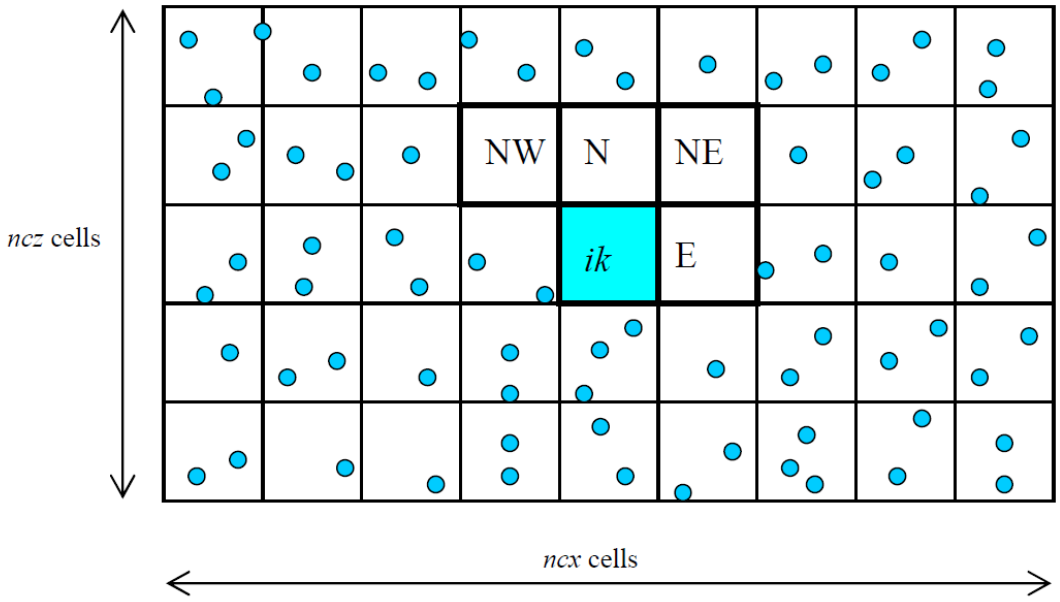

Figure 6: All particles are assigned to each cell, particles inside cell ik will only interact with adjacent cells of NW, N, NE and E from Gesteira et al, 2010 **[24]**.

2.2.6. Boundary Handling

Boundary treatment is always a major topic for applications of SPH. Usually, the boundary is made by putting one layer of particles, which also contributes to the calculation of interior particles. Comparing to grid-based methods, it's much easier to build structure with complex geometry. However, for the sake of accuracy, especially in relative small scale, attention has to be paid to the boundary treatment.

2.2.6.1. Stationary Boundary

A lot of methods have been proposed for stationary boundary. For example, Monaghan [54] uses stationary particle with repulsive force applying to fluid particle inside, which helps to prevent particles from penetrating the wall, but introduce unphysical noise into results; Libersky [60] introduces ghost particles outside boundary with the same field variable and calculate values of the interior particles with properties of ghost particles interpolated; for the studies by Liu [61] and Nadir [45], ghost particles also have the opposite velocity to the corresponding particles inside fluid region, which very similar to the technique used to treat no-slip boundary in grid-based method. Figure 7, extracted form A. Leroy 2014 [62] shows the sketch of these three major boundary molding techniques.

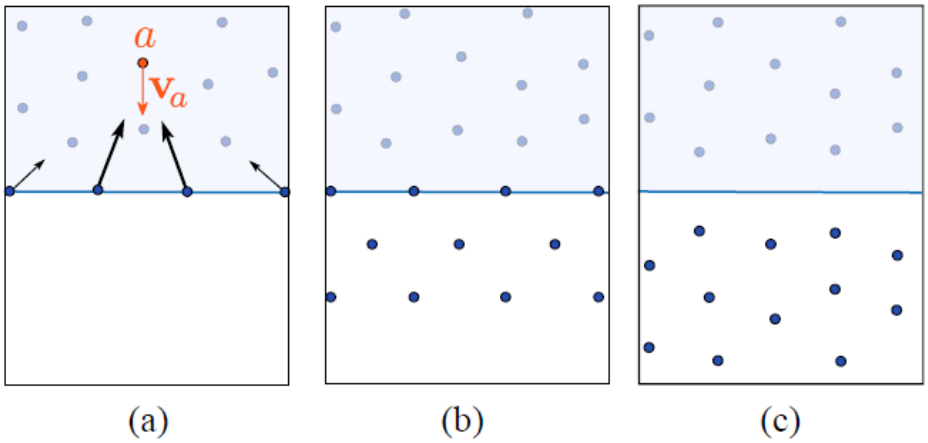

Figure 7: Sketch of three major wall boundary modelling techniques from A. Leroy 2014 **[62]**. (a) Repulsive boundary; (b) Stationary ghost particles; (c) Mirror particles.

In SPHysics, stationary ghost-particle model is applied with the same field variables. According to Eq. 7, as particle moving towards the boundary, the density will increase, and from Eq. 8 the pressure will also increase as in Figure 8, which will exerted an increasing force on this approaching particle to keep it from getting closer to the boundary. This mechanism provides a naturally anti-penetration boundary. Usually, 2-3 layers of ghost particle is enough to prevent any severe penetration of fluid particles. Besides the boundary particles have zero velocity, which mimics the effects of no-slip boundary condition.

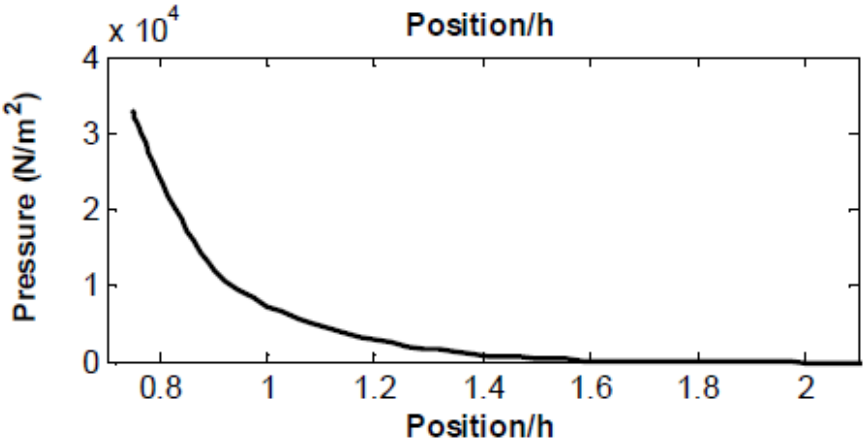

Figure 8: Variation of pressure for a moving particle approaching a solid boundary without viscosity calculation **[24]**

2.2.6.2. Periodic Boundary

Periodic boundary is one of the important boundary types for fluid dynamic simulation and is widely used in SPH simulations. It usually helps approximate a very large (infinite) simulation system to a small part. The idea of periodic boundary in SPH is: for particles near an open boundary,

the support domain will extend to the other side of the domain as shown in Figure 9. The periodic boundary also helps stabilize the system by avoiding free surface.

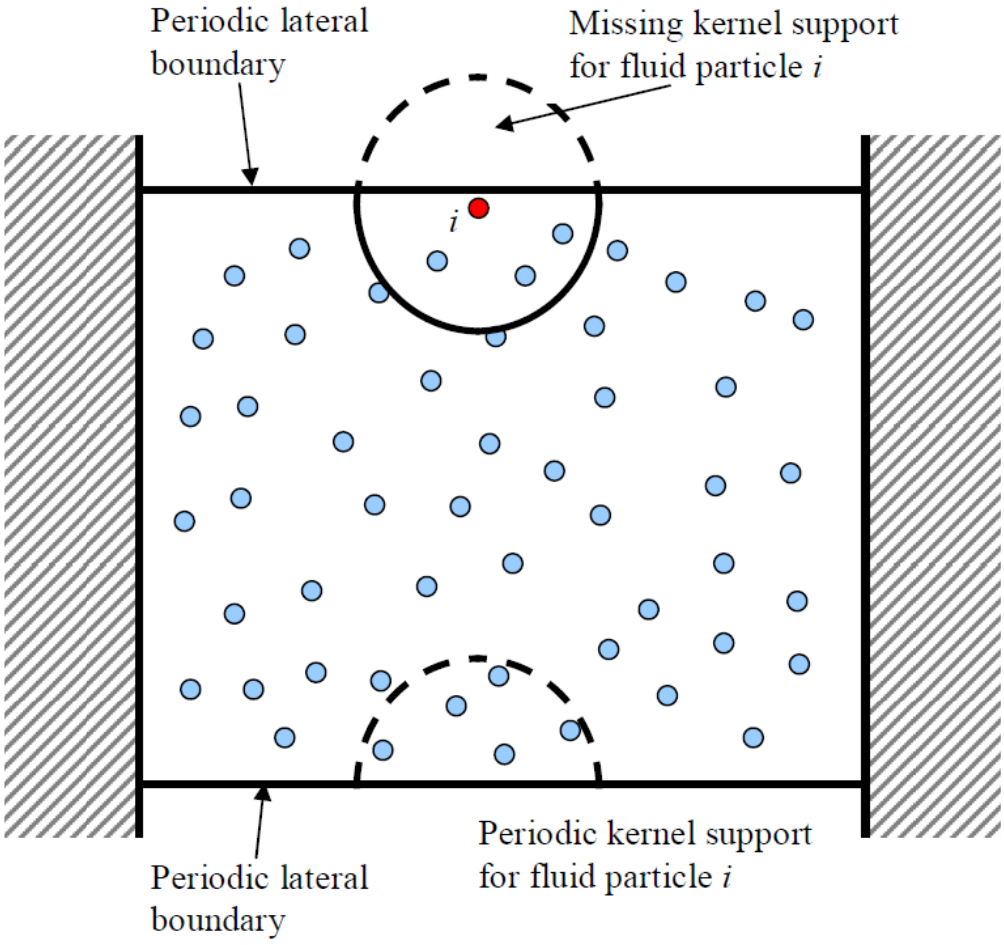

Figure 9: Mechanism of periodic boundary condition: the support domain of particle i extends beyond top boundary and continues through periodic bottom boundary **[24]**.

2.3. Micro-SPH Formulation

With the basic hydrodynamics properties inherited from SPHysics, it is capable of simulating incompressible/compressible flow with the effect of gravity and viscosity. More features related to micro-level simulation, like multiple shapes of surface structure, surface tension force, wettability model, interface tracking technique for multi-phase flow and so on are built into SPH code.

2.3.1. Surface Tension

In order to model the surface tension, techniques that can handle arbitrarily shaped interfaces between fluids is needed. Inherited from CSF methods proposed by Brackbill [63], for

immiscible fluids, different colors, c, are assigned to corresponding fluid and the interface can be tracked by simulating the advection of the color function [58].

$$\frac{\partial c}{\partial t} + \vec{v} \cdot \nabla c = 0 \qquad \text{Eq. 15}$$

In this work, the color function is naturally determined by density. Thus in SPH, color value of particle a is determined as:

$$c_a = \rho_a = \sum_b m_b \frac{1}{\rho_b} W(\overrightarrow{r_a} - \overrightarrow{r_b}) \qquad \text{Eq. 16}$$

The surface tension is accomplished with continuum surface force method. A transit region with finite thickness and fluid elements is applied to fluid interface. Thus the interfacial phenomena, such as surface tension and phase change, can be translated into volume processes that the net effects represent the real physics. For the case of interfaces between incompressible fluids with zero net viscous stress tensor and constant surface tension coefficient, the surface tension force can be written as [41]:

$$(\overrightarrow{F_s})_a = \sigma k \hat{n}_a |\vec{n}_a| \qquad \text{Eq. 17}$$

where $\hat{n}$ is the unit normal to the interface, σ is the surface tension coefficient, k is the curvature of the interface. The normal value of particle a can be obtained by

$$\overrightarrow{n_a} = \frac{\nabla c}{|c|} = \sum_b \frac{m_b}{\rho_b} [(c_s)_b - (c_s)_a] \nabla_a \overrightarrow{W_{ab}} \qquad \text{Eq. 18}$$

where c is the color function identifying each fluid and $|c|$ is the jump of c across the interface. Then curvature of particle a can be determined by

$$k_a = -\nabla \cdot \hat{n} = -\sum_b \frac{m_b}{\rho_b} (\hat{n}_b - \hat{n}_\mathrm{a}) \cdot \nabla_a \overrightarrow{W_{ab}} \qquad \text{Eq. 19}$$

2.3.2. Surface Adhesion (Wettability)

Wettability effects can be considered as the result of competes of attraction force among fluid particles themselves against the attraction between fluid and boundary particle, which will need a new model. We present two different wettability model based on Nadir [45] and Meakin [64]'s work.

1. Fourth order attraction force

The wettability effect is mimicked by applying additional adhesion force between surface and fluid particles. The adhesion force has the expression of

$$F_{ij} = -\beta m_j m_i A(r) \frac{\vec{r}}{|\vec{r}|} \qquad \text{Eq. 20}$$

where A is spline function based on Nadir's work [45] for 2D case:

$$A(r) = \frac{0.007}{h^{2.25}} \begin{cases} \sqrt[4]{-\frac{4r^2}{h} + 6r - 2h}, & \frac{h}{2} < r \leq h \\ 0, & elsewhere \end{cases} \quad \text{Eq. 21}$$

where $h^{2.25}$ is to make integral of $A(r)$ to be the same for different support radius h, while 0.007 is selected such that β values is similar to γ (surface tension coefficient). The shape of this kernel function is shown:

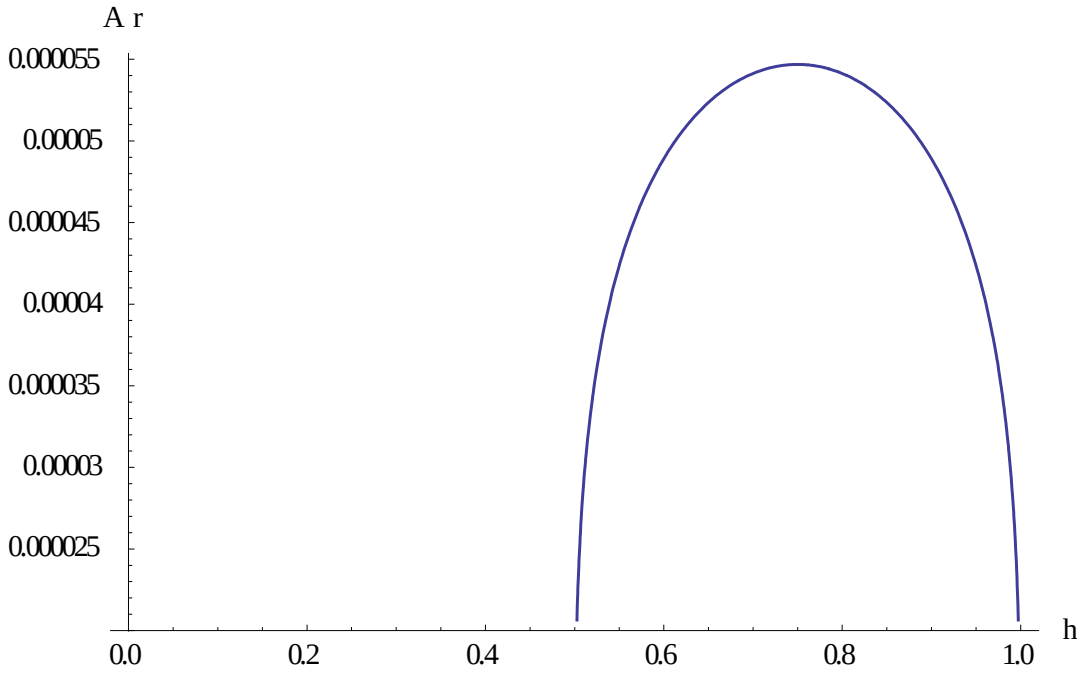

Figure 10: Shape of adhesion function with support radius h = 1.

2. Attraction force of "Lennard-Jones Potential" form

The second model of wettability is based on Lennard-Jones potential form, a similar mathematic formula is proposed to mimic the effect of particles' attraction and repulsion force. The model can be represented as:

$$F_{i \leftarrow j}^{adhesion} = -\beta m_i m_j A\,(|x_i - x_k|)\frac{x_i - x_j}{|x_i - x_j|} \quad \text{Eq. 22}$$

where C is the kernel of the adhesion function

$$A(r) = \frac{32}{\pi h^9}\begin{cases} (h-r)^3 r^3, & h \geq r > h/2 \\ 2(h-r)^3 r^3 - \dfrac{h^6}{64}, & h/2 \geq r > 0 \\ 0, & elsewhere \end{cases} \qquad \text{Eq. 23}$$

The shape of this formula can be plotted as:

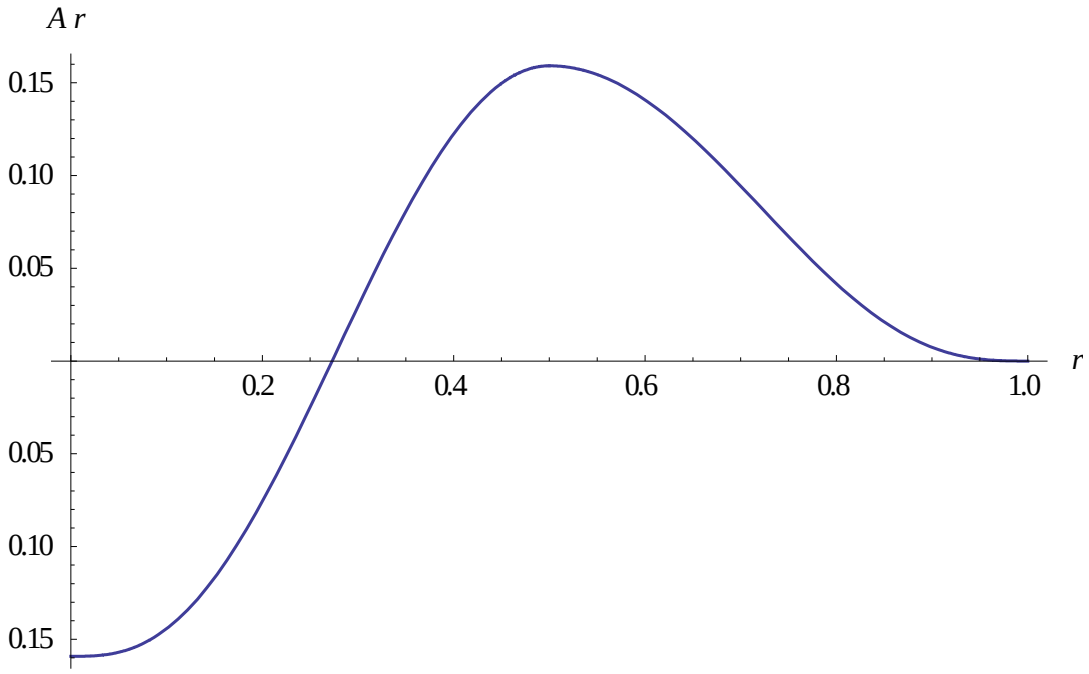

Figure 11: Shape of adhesion function with support radius h=1.

2.3.3. Multi-Fluid Interface Generation

The interface generation is achieved by setting limit for the color value determined during the surface tension calculation. Particles with color value lower than the limit is treated as boundary.

2.3.4. Other (missing) Physics

Though capillarity force is covered in this program, some key physics are still missing. Phenomena like heat transfer and phase change still need more development for the micro-hydrodynamics study. As for flooding, dynamics like turbulence, tornado is still missing.

2.3.5. Post-Processing

Most post-processing of this study is done by Matlab, which will read and analyze the data output. Because comparison between the results from SPH and grid-based methods is needed, a transfer algorithm of distributing particle properties to each grid is constructed. The idea of Euler method is to average the properties over the mesh, same thinking is applied here: mesh is constructed over the computational/investigational domain, then all particles within each cell are

found and simple averages, as indicated in Eq. 22, are taken for the properties carried by these particles as shown in Figure 12.

$$f_{i-cell} = \sum_{k=1}^{N} f_{k-particle} \qquad \text{Eq. 24}$$

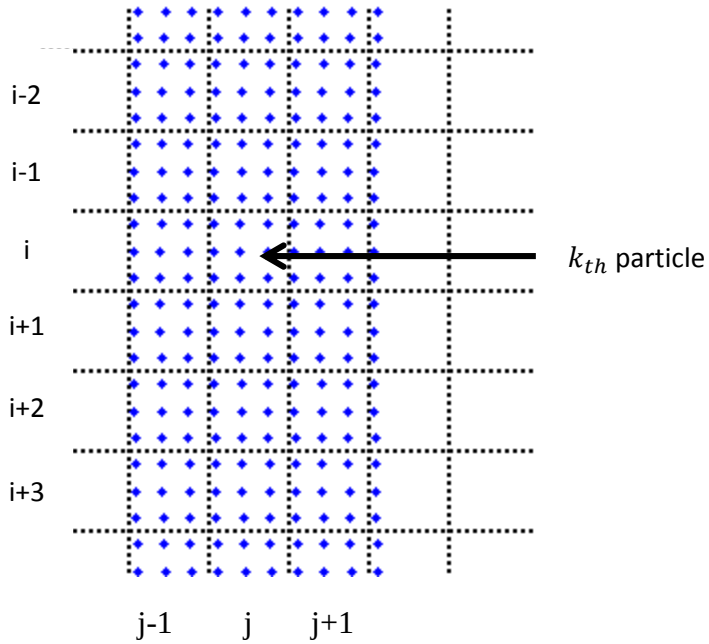

Figure 12: Distribution of uniform grid and SPH particles. Total of N particles lays inside cell ij.

2.4. Non-dimensional Formulation

Non-dimensionalization is the removal of units from the equations by introducing scale variables. The non-dimensional study is important for physical scaling and revealing system properties. In this study, variables listed in Eq. 25 are introduced, where L is length scale, T is time scale, ρ is reference scale and f is force scale.

$$r^* = r/L, \quad t^* = t/T, \quad \rho_a^* = \rho_a/\rho, \quad \vec{f}^* = \vec{f}/f, \quad v^* = v/U$$
$$U = L/T, \quad h^* = h/L, \quad m^* = m/\left(\rho L^3\right) \qquad \text{Eq. 25}$$

Then the non-dimensional form of cubic kernel function is found to be:

$$W_{ab}^* = \frac{1}{\pi\left(h^*\right)^3}\begin{cases} 1-\frac{3}{2}q^2+\frac{3}{4}q^3 & 0 \le q \le 1 \\ \frac{1}{4}(2-q)^3 & 1 < q \le 2 \\ 0 & 2 < q \end{cases} \qquad \text{Eq. 26}$$

And the continuity (Eq. 7) and momentum equation (Eq. 10 & Eq. 14) can be determined as:

$$\frac{D\rho_a^*}{Dt^*} = \sum_b m_b^* \vec{v}_{ab}^* \vec{\nabla}^* W_{ab}^*$$

$$\frac{1}{Sl}\frac{D\vec{v}_a^*}{Dt^*} = \sum_b m_b^* \left(\frac{P_b^*}{\left(\rho_b^*\right)^2} + \frac{P_a^*}{\left(\rho_a^*\right)^2} \right) \vec{\nabla}^* W_{ab}^* + \sum_b m_b^* \left(\frac{1}{\mathrm{Re}} \frac{4\vec{r}_{ab}^* \vec{\nabla}^* W_{ab}^*}{\rho_b^* + \rho_b^* \left|\vec{r}_{ab}\right|^2} \right) \vec{v}_{ab}^* + \frac{fL}{U^2} \vec{f}^* \quad \text{Eq. 27}$$

Furthermore, the non-dimensional surface tension force can be determined as:

$$\left(\vec{f}_{curv}^*\right)_a = \frac{U^2}{L} \left(\frac{1}{We} \frac{1}{\rho_a^*} k_a^* n_a \left| \vec{n}_a^* \right| \right) \quad \text{Eq. 28}$$

where $k^* = Lk$ and $n^* = Ln$, ∇^* denotes the gradient operator with respect to the dimensionless coordinate r^*. Sl, Re and We is the Strouhal, Reynold and Weber number respectively and they are defined by:

$$Sl = \frac{UT}{L}, \qquad \mathrm{Re} = \frac{\rho LU}{\mu} = \frac{LU}{\nu}, \qquad We = \frac{\rho LU^2}{\gamma} \quad \text{Eq. 29}$$

2.5. Stability and Time Step

To ensure the numerical stability, Courant-Friedrichs-Levy (CFL) is applied to ensure time-step remains lower than the maximal convection time on the smoothing length h during the simulation as shown in Eq. 30.

$$\Delta t = min\left(0.25\frac{h}{c}, 0.125\frac{\rho h^2}{\mu}, 0.25\left(\frac{\rho h^3}{2\pi\sigma}\right)^{\frac{1}{2}}, 0.25 \min_b \left(\frac{h}{a_b}\right)^{\frac{1}{2}} \right) \quad \text{Eq. 30}$$

The four criteria represent conditions due to sound waves, viscous diffusion [57], capillary wave phase velocity [63] and individual particle accelerations [54] respectively.

3. Code and Solution Verification

Guided by the PIRT process and flow chart shown in Figure 5, test cases listed in Table 5 are performed and results are evaluated by comparing them either to analytical solutions and numerical outputs from fine-mesh methods, or directly to experimental measurements. Note that in lid-driven cavity flow, vortex shedding and 3D dam break problem, NEUTRINO [44] is applied because of the relatively large number particles (~1 million) involved. As NEUTRINO only applies a similar solving strategy of hydrodynamics to Micro-SPH, these results can server as a supplementary assessment of certain features in SPH.

3.1. Internal Flow

The Poiseuille Flow simulation verifies the model's viscosity model and boundary by showing the error against analytic solution and the convergence with the mesh refine.

3.1.1. Poiseuille Flow

The Poiseuille flow investigates the flow between two parallel infinite plates (at x=0 and x=l). The fluid between is driven by a body force to represent the constant pressure difference. The flow will finally arrive at a steady state. Morris [57] provided a series solution for the time dependent behavior of the Poiseuille flow:

$$u_x(y,t) = \frac{F}{2\nu} y(y-l) + \sum_{n=0}^{\infty} \frac{4Fl^2}{\nu\pi^3(2n+1)^3} sin(\frac{\pi y}{l}(2n+1)) exp(-\frac{(2n+1)^2\pi^2\nu}{l^2}t) \quad \text{Eq. 31}$$

In this study, $l = 10^{-3}m$. $\rho = 10^3 kg/m^3$, the kinetic viscosity $\nu = 10^{-6}m^2/s$, and the driven body force acceleration is $F = 2 \times 10^{-4}m/s^2$. According to equation Eq. 31, the peak fluid velocity is $u_0 = 2.5 \times 10^{-5}m/s$, which corresponds to the Reynolds number of $Re = 2.5 \times 10^{-2}$. In this simulation, periodic boundary condition is applied to save time. 20×40 particles are simulated on a rectangular domain of $0.0005m \times 0.0001m$. Figure 13 shows the particle distribution and velocity quiver plot at t = 0 and t =1. We can see some particles originally locating at downstream goes to upstream because of the periodic boundary condition. Figure 14 shows the comparison between the velocity profiles obtained using SPH methods and those by Eq. 31. Figure 15 shows the development of maximum speed versus time for this simulation, which will reach equilibrium velocity as Eq. 32 predicted. L^2 Relative error norm is defined to determine the relative error of SPH results against analytical solution [65] and a good agreement is found with maximum L^2 error to be 0.8%. Figure 16 shows the plot of L^2 error against particle size. Because a differential equation is solved in this study, convergence of error with decreasing of particle size is expected. The relative error is plotted with particle size and compared to 1st and 2nd order convergence line from Fatechi et al, 2011 [66]'s work, in which the error is calculated as the difference between SPH particle approximation and the Tylor series expansion up to 1st and 2nd order of velocity.

$$L^2\ relative\ error\ norm = \sqrt{\frac{\sum_{i=1}^{i=N}\left(u_{SPH}(i)-u_{Exac}(i)\right)^2}{\sum_{i=1}^{i=N} u_{Exact}^2(i)}} \qquad \text{Eq. 32}$$

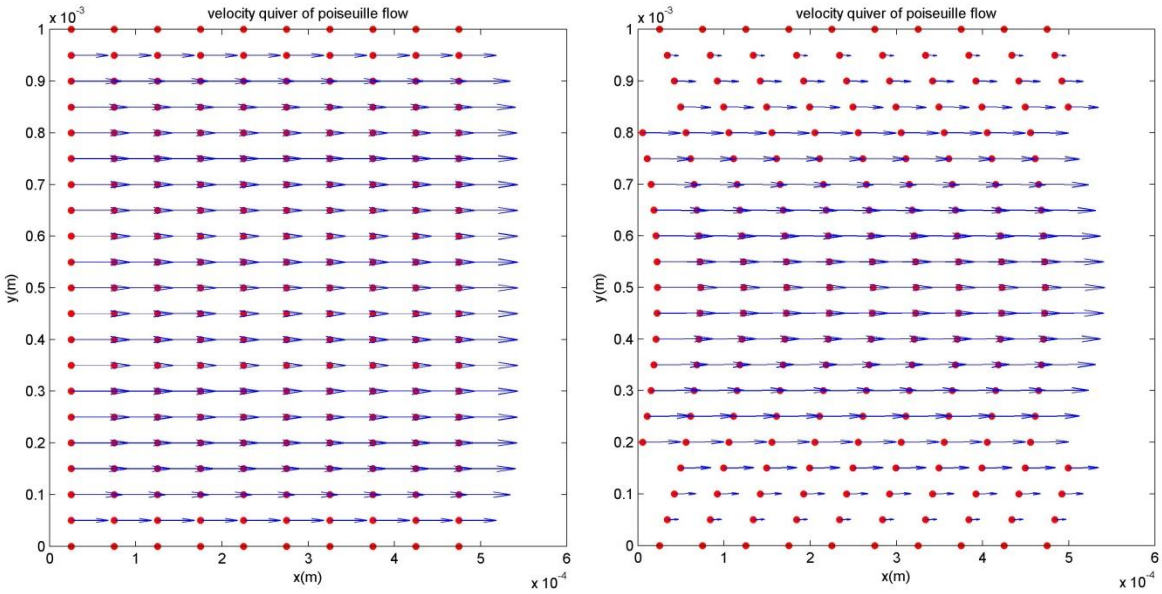

Figure 13: Velocity quiver for the Poisuille flow at initial time (t=0) and stable states (t=1sec).

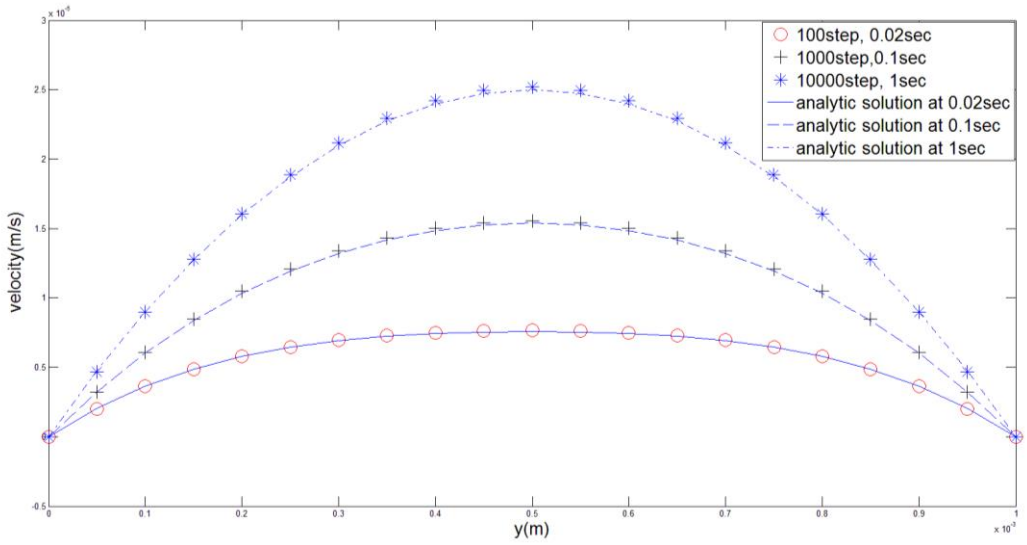

Figure 14: Comparison of velocity profile from SPH to analytic solution for the Poiseuille flow.

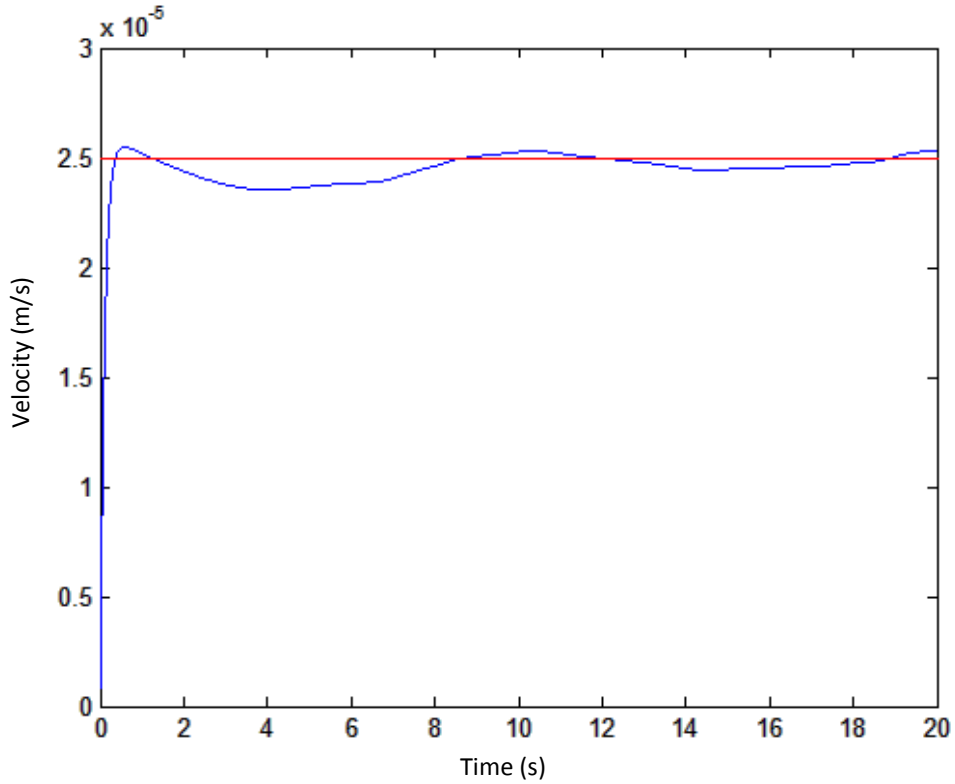

Figure 15: The development of maximum velocity in Poiseuille flow with time.

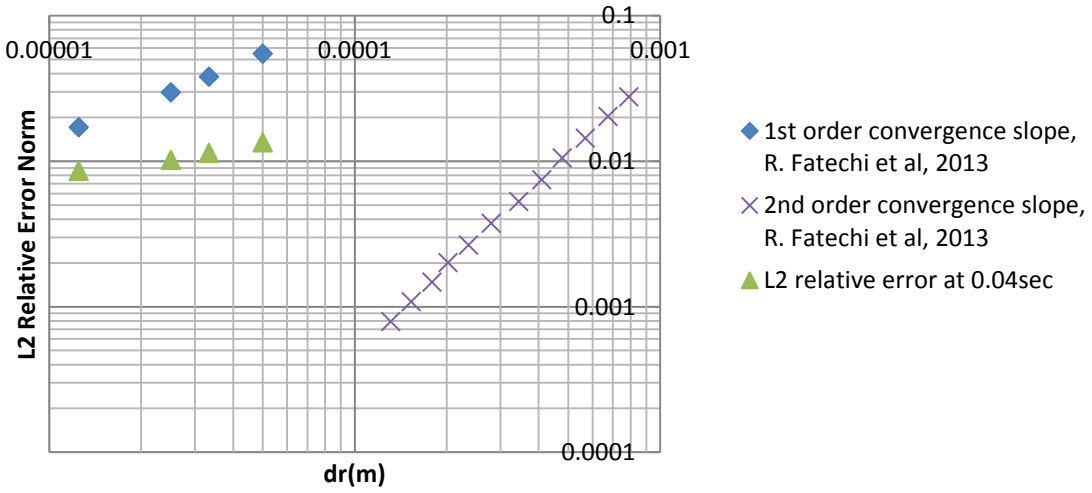

Figure 16: Plot of $\boldsymbol{L^2}$ error to particle size compared to 1st and 2nd order convergence line from R. Fatechi et al, 2011 **[66]**.

It can be noticed that the convergence rate of our simulation is higher than the second order and it indicates some high order error is involved in our simulation. As indicated by A. Leroy, 2014 [62] and S. Shahriari et al, 2011 [65]'s work, this could possibly due to the artificial compressibility term.

3.1.2. Lid-Driven Cavity Flow

The lid-driven cavity flow investigate the fluid flow within a closed square and move the top side of the square at a constant velocity while the other three sides remain stationary. The flow will reach a steady state. In this simulation, a 2D square with $l = 10^{-3}m$ and top layer speed $u_{Top} = 10^{-3}m/s$. A total number of 1521 fluid particles are simulated. The initial and final particles distributions are shown in Figure 18. A comparison between results from SPH and Finite Difference Methods (FDM) is made for non-dimensional horizontal/vertical velocity profile along the vertical/horizontal centerline. As shown in Figure 19, the results from two methods agree well.

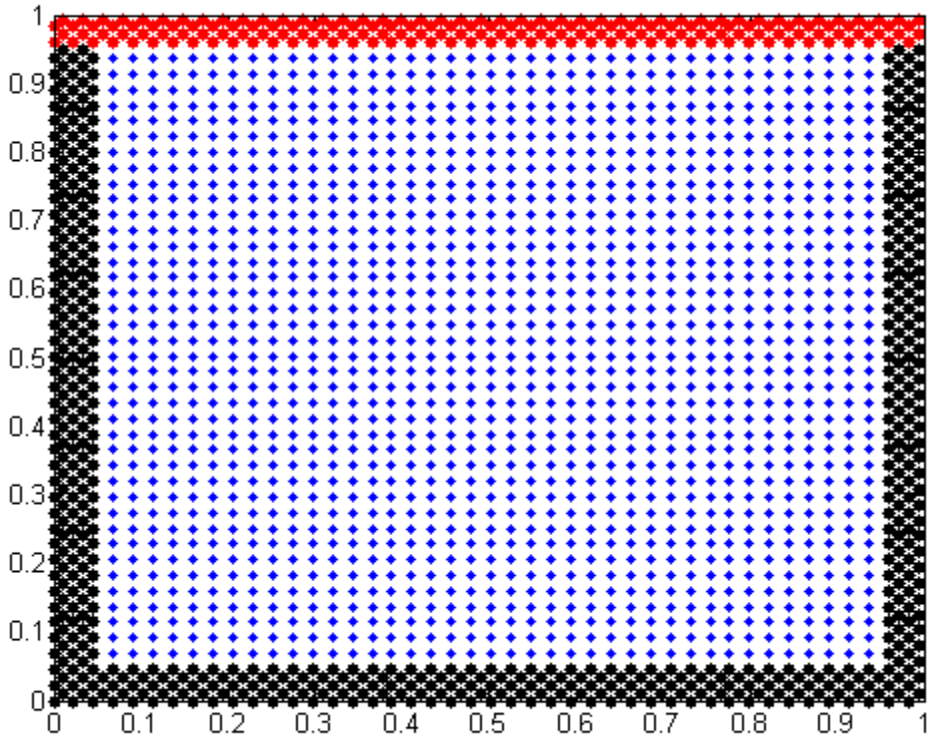

Figure 17: Plot of initial setup with red particles as driven particles with speed$\boldsymbol{10^{-3}m/s}$, blue as fluid particles, and black as no-slip boundary particles.

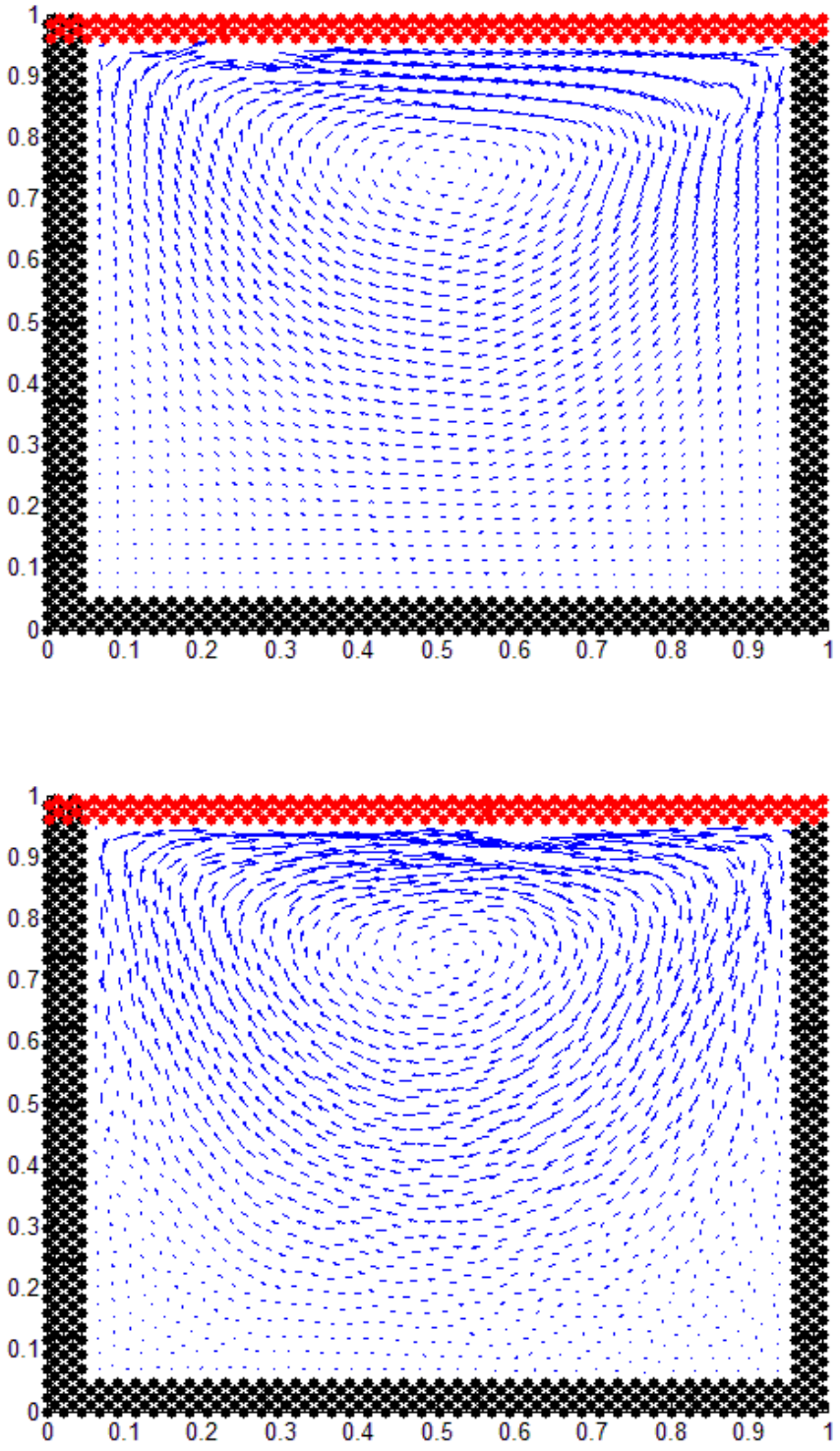

Figure 18: Velocity quiver plot of fluid particles at 0.05sec (top) and final steady states at step 0.4sec (bottom).

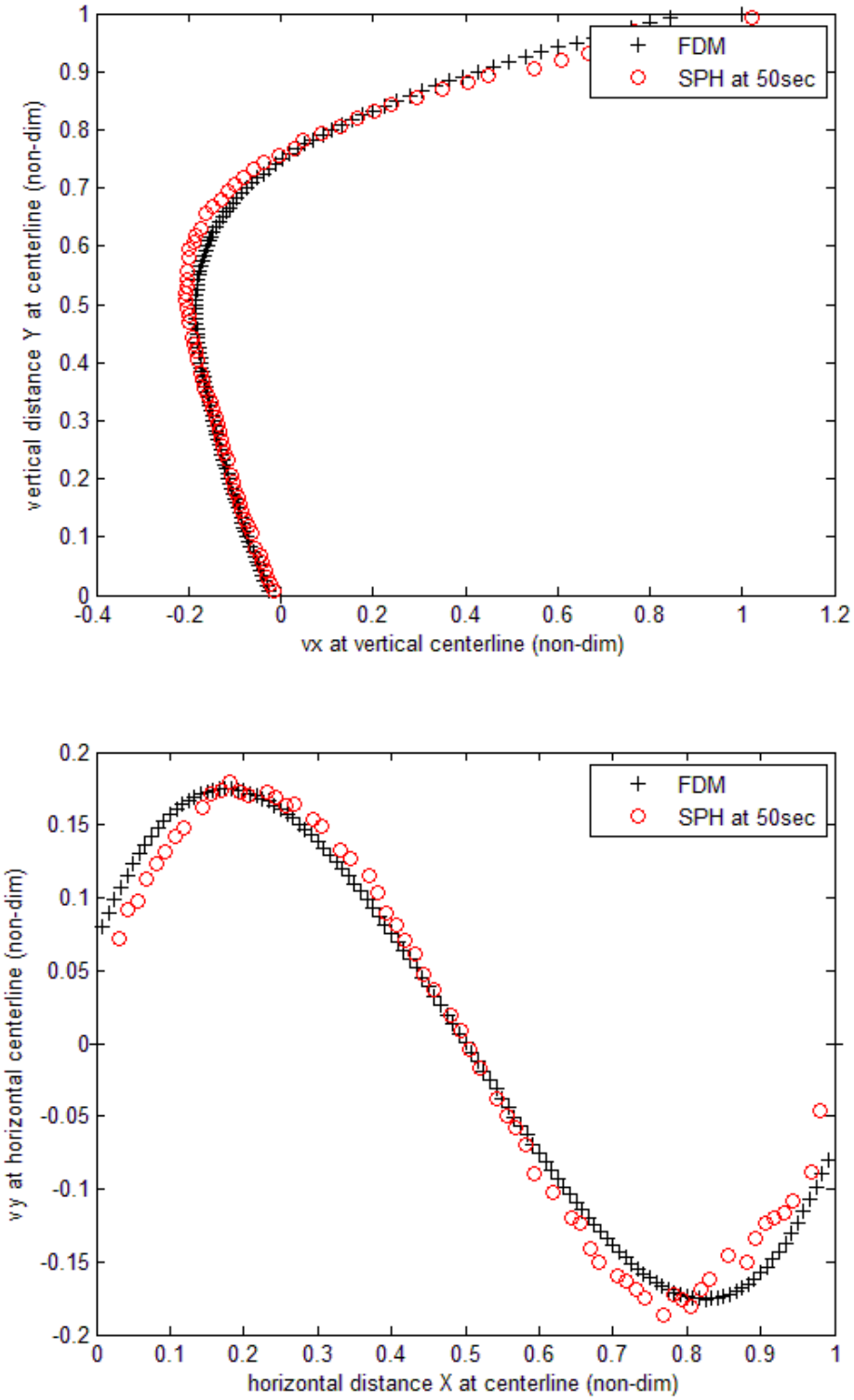

Figure 19: Comparison of results from SPH and FDM for non-dimensional vertical velocities along the horizontal centerline (upper) and horizontal velocities along the vertical centerline (lower) at 50sec as steady state.

It's noticed that some discrepancy exists between SPH simulation and fine-mesh simulations, which could be caused by the artificial compressibility terms. Figure 20 shows the comparison of pressure distribution along the diagonal and horizontal centerline. The trend for diagonal looks similar, but the other plot is dominated by pressure fluctuations as mentioned in section 2.4. This also explains the distribution of horizontal velocity v_x is more accurately predicted than vertical velocity v_y.

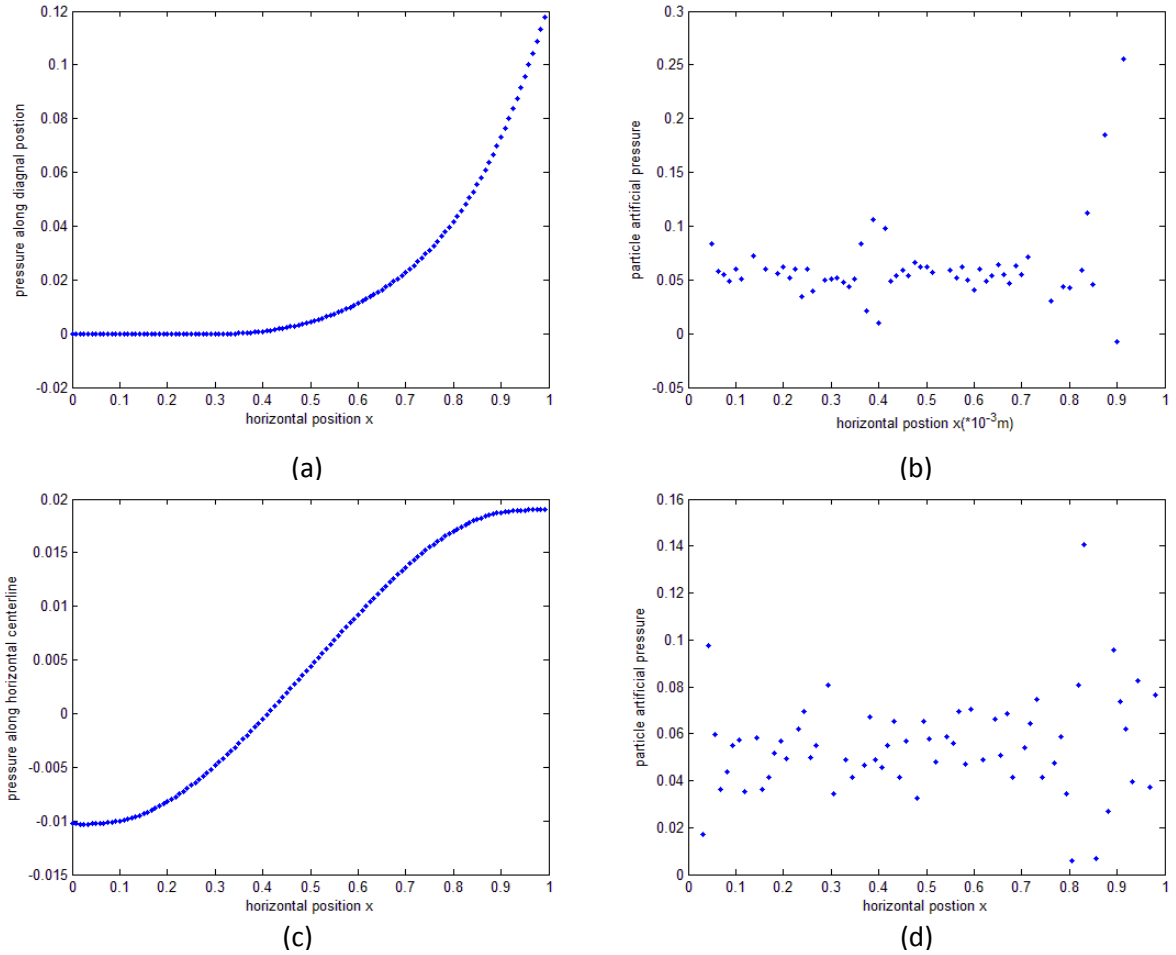

Figure 20: Comparison of pressure distribution along the diagonal line (upper) from fine-mesh (a) and SPH (b), and along the horizontal centerline (lower) from fine-mesh (c) and SPH (d).

As Reynold number increasing, issue of particle vacancy may become important. Due to the nature of weakly-compressed formula, particles with high speed tends to squeeze and leave vacancy behind. Figure 21 (a) shows the particle distribution at Re = 100. Though the result looks still accurate in (b), but the number of particles found as upper level increases a lot compared to Figure 19. The deficiency could become severe as Reynolds number is increased further, shown in Figure 22, and SPH is known to have accuracy problem at low density position where the number of particles is few.

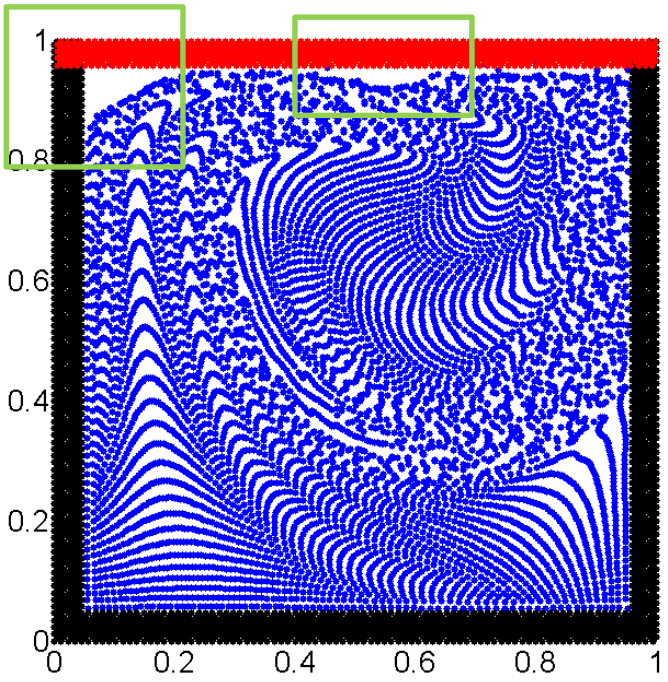

(a)

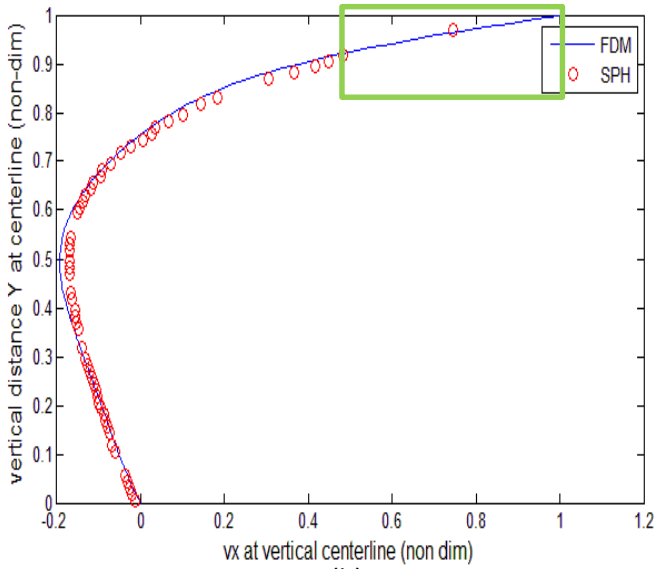

(b)

Figure 21: Particle distribution plot (a) and horizontal velocity distribution (b) along horizontal centerline with Re = 100 at t = 0.05s. Areas inside green boxes show a particle deficiency problem where very few particles are found.

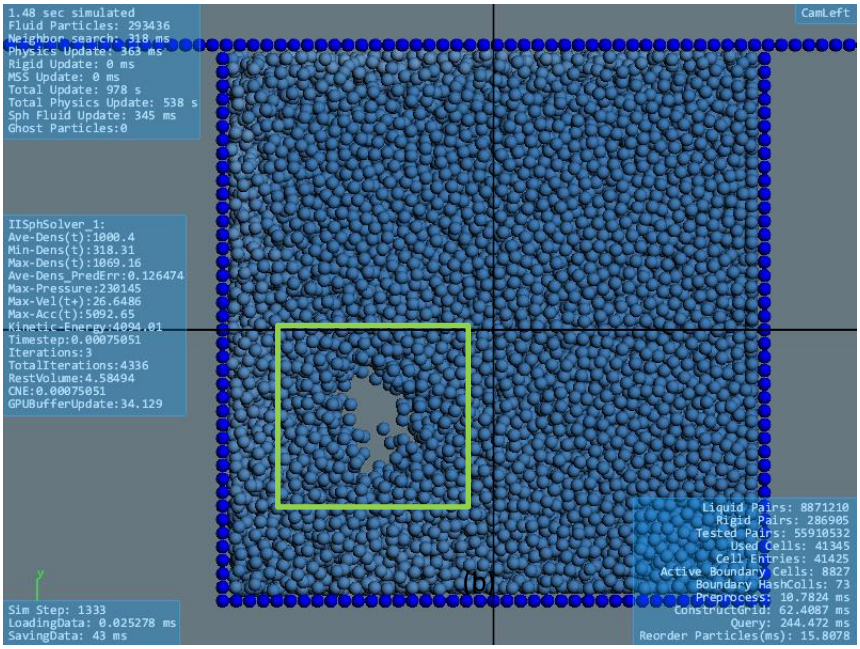

Figure 22: Lid-driven flow simulated by Neutrino **[44]** with Re = 1.2E5 and 1E5 particles, apparent vacancy is found as marked inside the green box.

3.2. External and Free Surface Flow

3.2.1. Flow around Cylinder

3.2.1.1. Low-Reynold Number Simulation

Flow around cylinder for low Reynolds Number ($Re = 1$) is simulated using parameter and periodic boundary condition as suggested by Morris [57], Figure 23 shows the initial setup of the problem and Figure 24 shows the velocity quiver plot at transient and final stable time point. The fluid particles are marked as blue and the solid cylinder is marked as red.

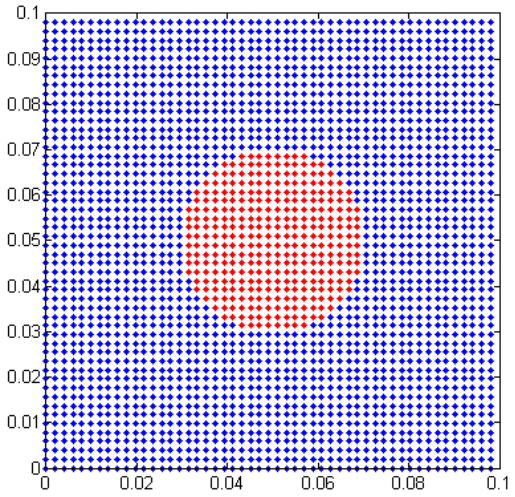

Figure 23: Initial setup (top) of fluid particles (blue) and cylinder (red), the left and right boundary is periodic, while the top and bottom layers are non-slip boundary.

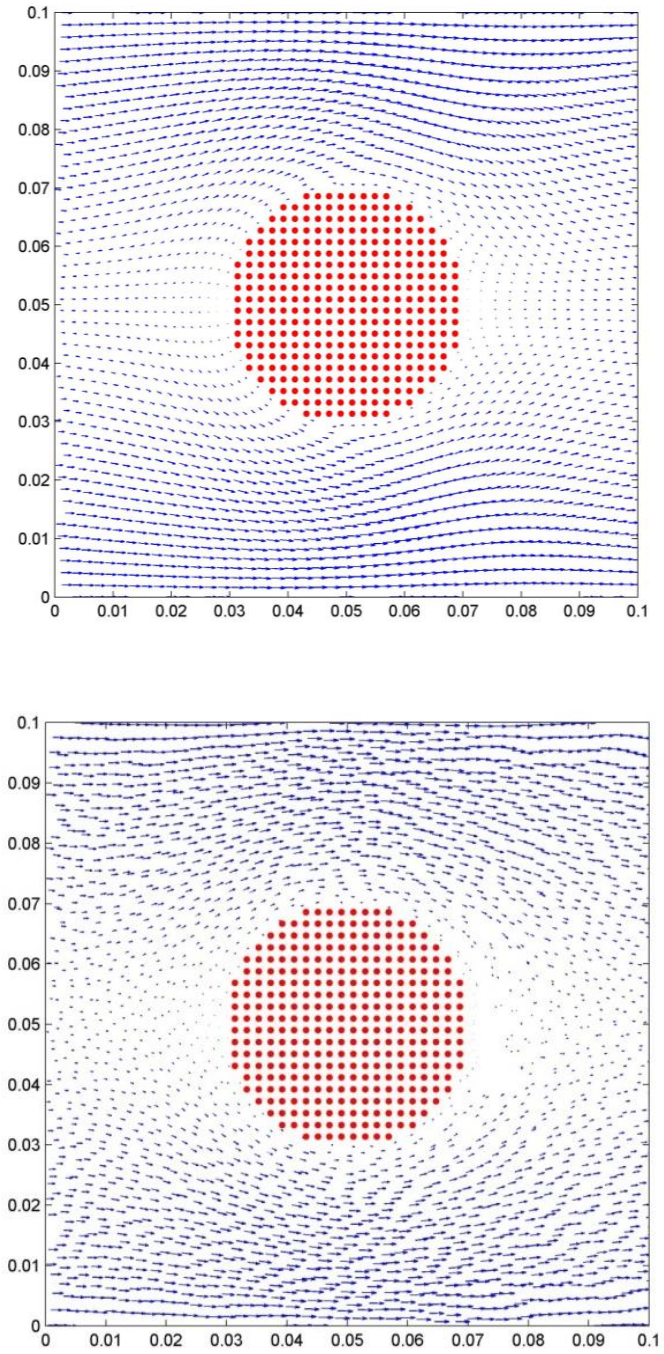

Figure 24: Quiver velocity plot of fluid particles at (1) 480sec (first step) (3) 7500sec (stable state).

Also the velocity quiver plot is shown. Figure 26 shows the velocity profile along two paths 1 and 2, shown in Figure 25, from Morris's paper and from SPH simulation, a good agreement is found between simulation results and reference data.

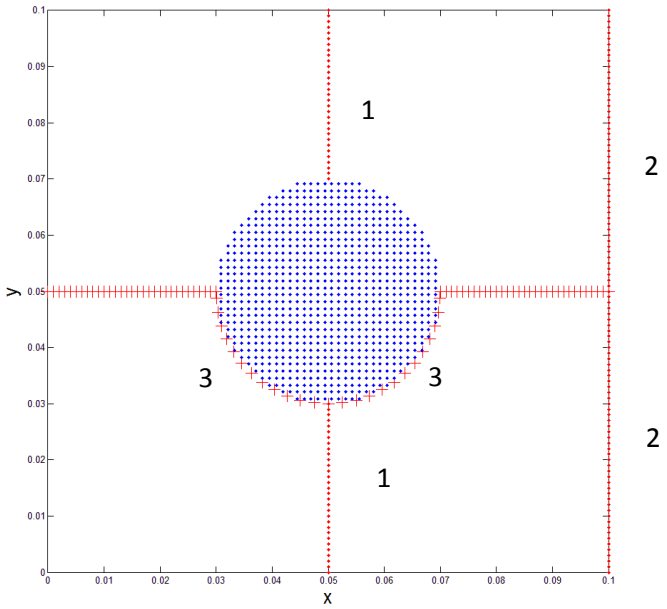

Figure 25: Paths for comparison of SPH with results from Morris et.al 1997 **[58]**.

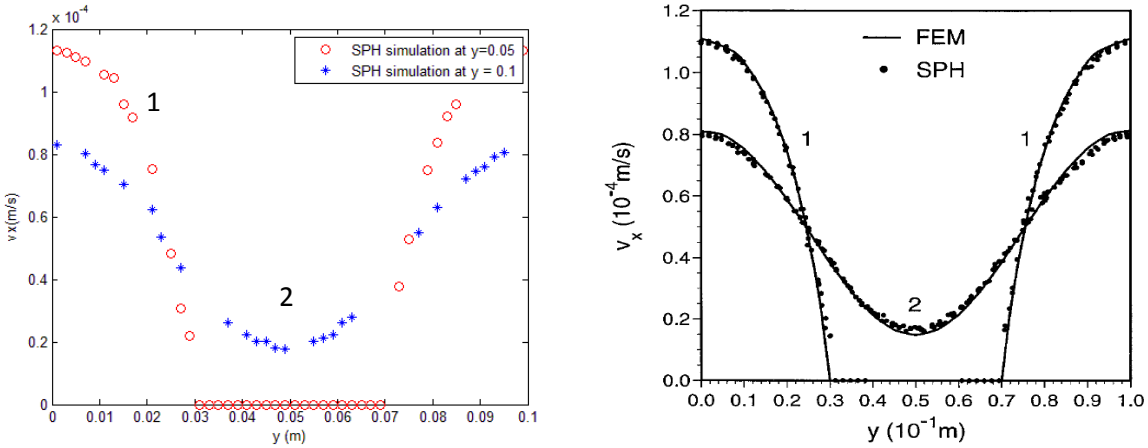

Figure 26: Comparison of SPH's velocity profiles along paths 1 and 2 at y =0.05 and y = 0.1 with Morris et al, 2000 results **[58]**.

Figure 27 shows the comparison of pressure distribution along path 3 from SPH and Morris's work. The trends are similar but magnitudes are different. This is due to the high order artificial compressibility term, where a small change in density will result in large fluctuation in pressure. It will make the pressure unlikely to be zero even during steady state.

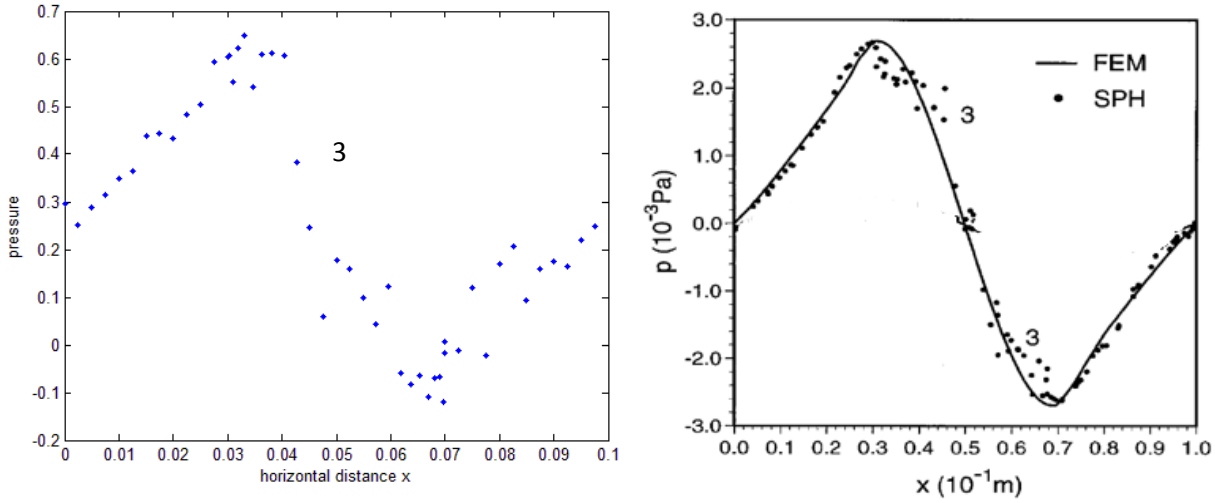

Figure 27: Comparison of pressure from SPH and Morris et al, 1997 **[58]** along path 3.

3.2.1.2. Vortex Shedding

In the flooding scenario, lots of solid structures will stand on the flow path. The flow pattern behind the structure will be an important feature to measure. The vortex shedding is expected to be seen when fluid flows past a bluff body at certain velocities. Vortices are created at the back of the body and detach periodically from either side of the body. Because accuracy is an important concern for SPH when comparing to mesh-based methods, the finding of vortex, as shown in, Figure 28 (a), is a good validation cases for SPH. Also from (b) it can be noticed that particle size has a significant effect on the accuracy. When the particle size is doubled, no vortex shedding can be found.

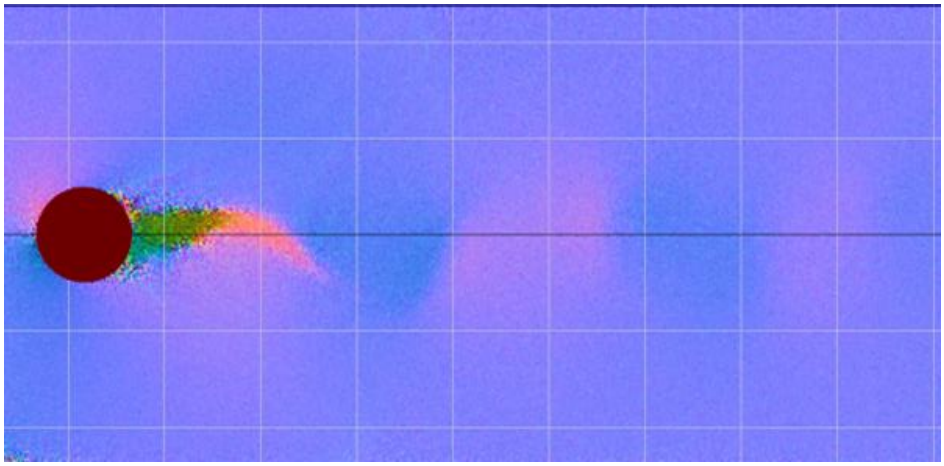

(a)

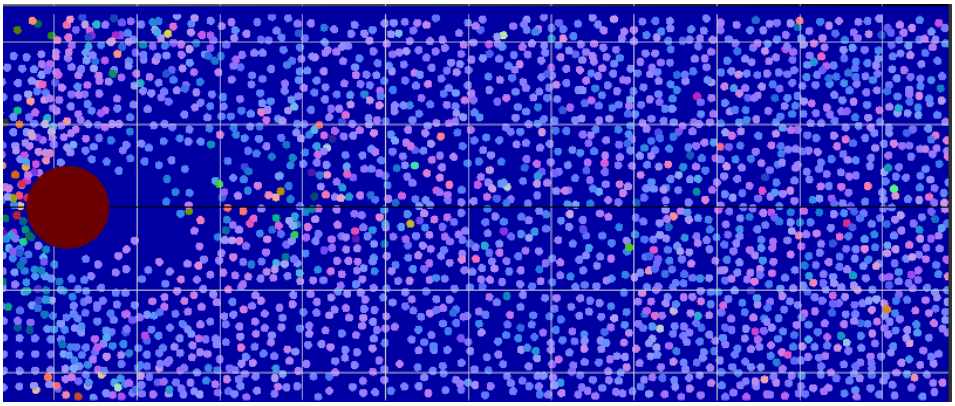

(b)

Figure 28: Vortex shedding after flow pass cylinder from Neutrino **[44]** with particle size = 0.05, 2×10^6 particles at fully developed state (a) and 0.1 (b), information is missing with coarse particle size.

3.2.2. Dam Breaking

Dam break is simulated by most of SPH program to demonstrate the SPH's power of dealing free-surface slamming phenomena, it's also important for the measurement of force exerted from fluid to the solid structures. Both two features are key parameters for the flooding simulations. Here two tests are run for the flooding scenario, the collapse of water column is main for investigating the free surface movement, while the 3D dam breaking is for measuring the force acting onto the solid structure. Both simulation results are compared with experimental data to show the capability of SPH in doing flooding simulation.

3.2.2.1. Collapse of Water Column

The collapse of water column is a typical test for SPH, it shows the advantage of SPH when dealing with free surface. In this case, a water column is put in a rectangular container as shown

in Figure 29. The simulation result is compared to experimental data done by S. Koshizuka [67] and Martin [68] as shown in Figure 31.

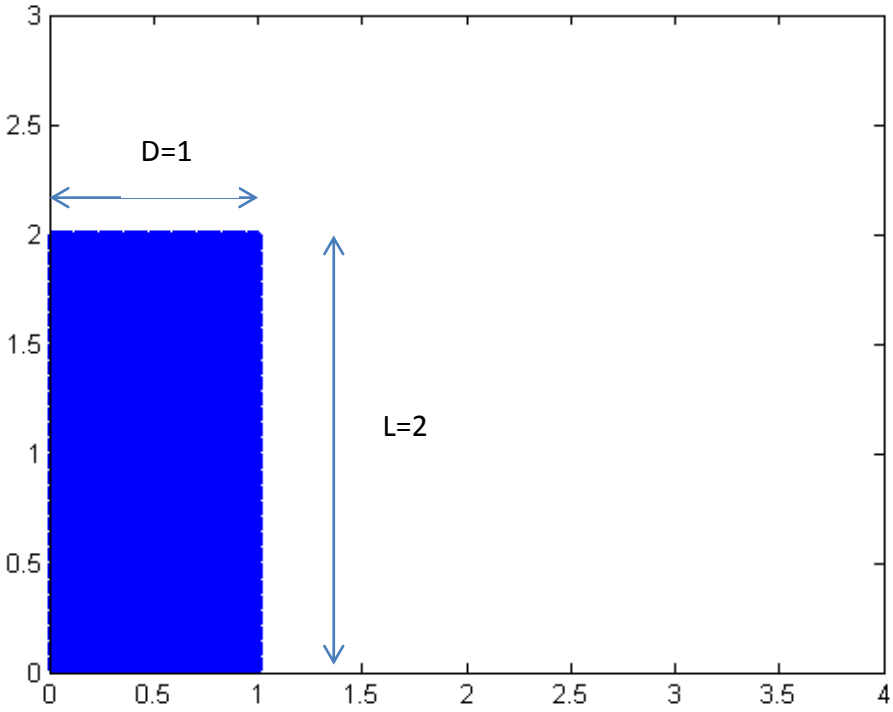

Figure 29: Initial setup of water column collapse and letter representation of geometric parameter D & L

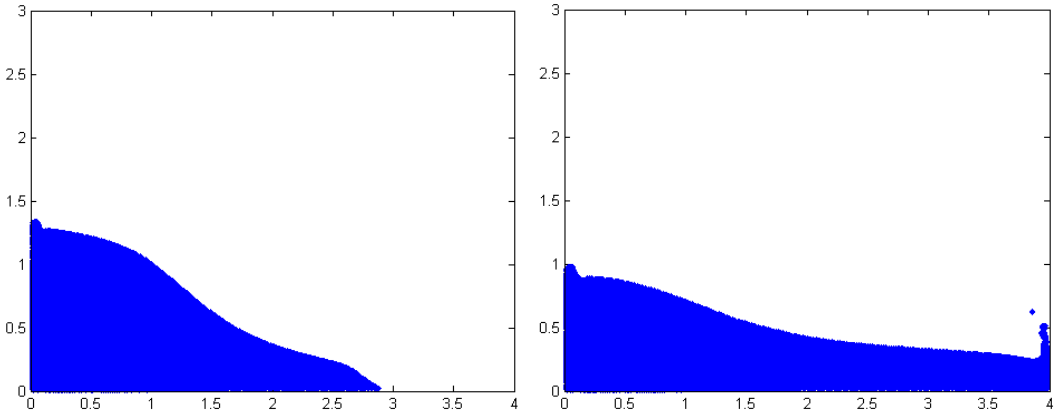

Figure 30: SPH simulated water collapse at 0.5sec and 0.72sec.

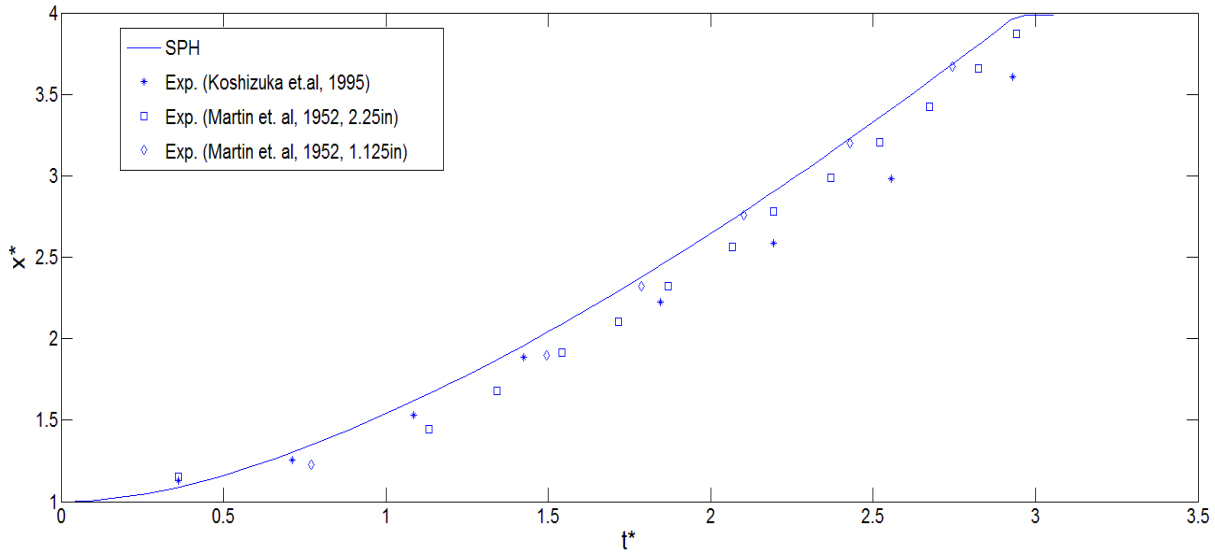

Figure 31: Comparison of SPH simulation results with experimental data by S. Koshizuka **[67]** and J.C. Martin [49].

where x* is the dimensionless position of the water front and t* is the dimensionless time defined as:

$$x^* = x/D \quad \text{Eq. 33}$$

$$t^* = t\sqrt{2g/D} \quad \text{Eq. 34}$$

The calculated result is almost the same as the experimental data and this shows good capability of SPH doing free surface problem.

3.2.2.2. Force Acting on Dam Structure

In this case, SPH flooding software, NEUTRINO [44], is used for the validation purpose because of a large number of particles are involved (60K ~ 120K). We measure the force exerted by fluid particles onto the dam structure and compare the results with experimental data. The simulation is one-to-one scale to real experiments and set up as in Figure 32 according to Cummins work [69]. In NEUTRINO, a gate is first put in position and held for 1 sec until all fluid particles are settled down. Then the gate is opened and fluid collapses driven by gravity. Figure 33 shows the evolution of fluid over the surface.

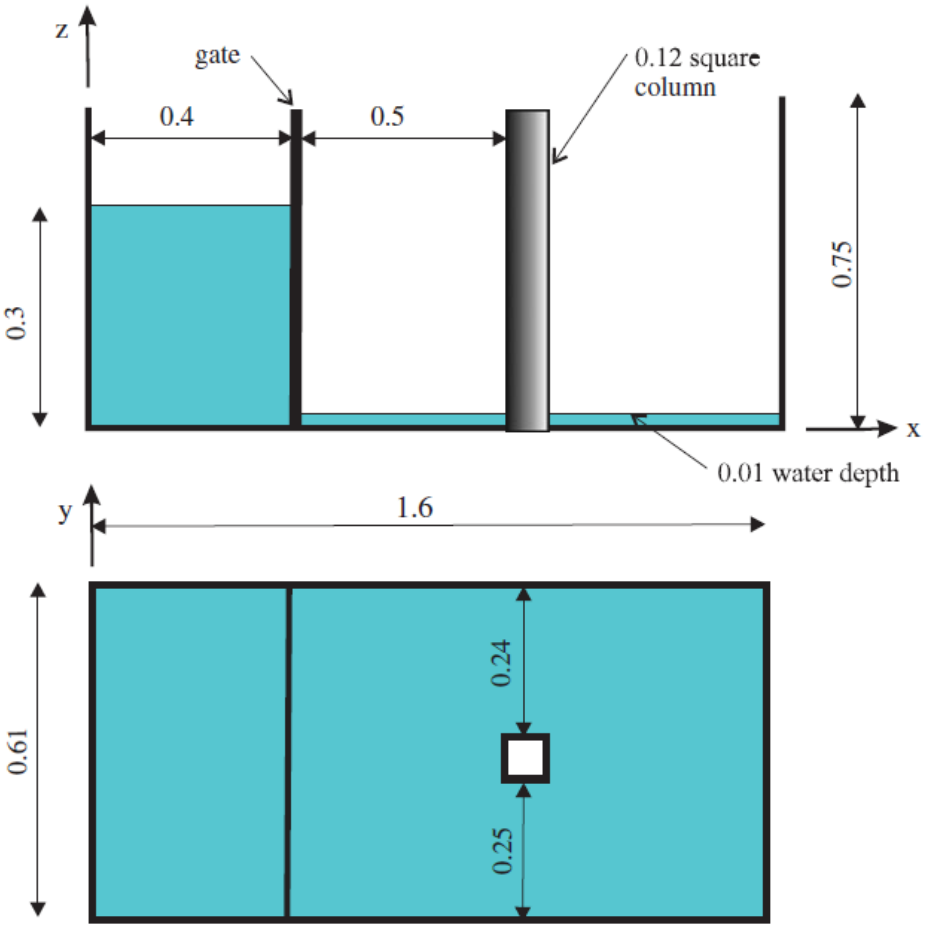

Figure 32: Schematic diagram of the dam geometry from Cummins et al. 2012 [50].

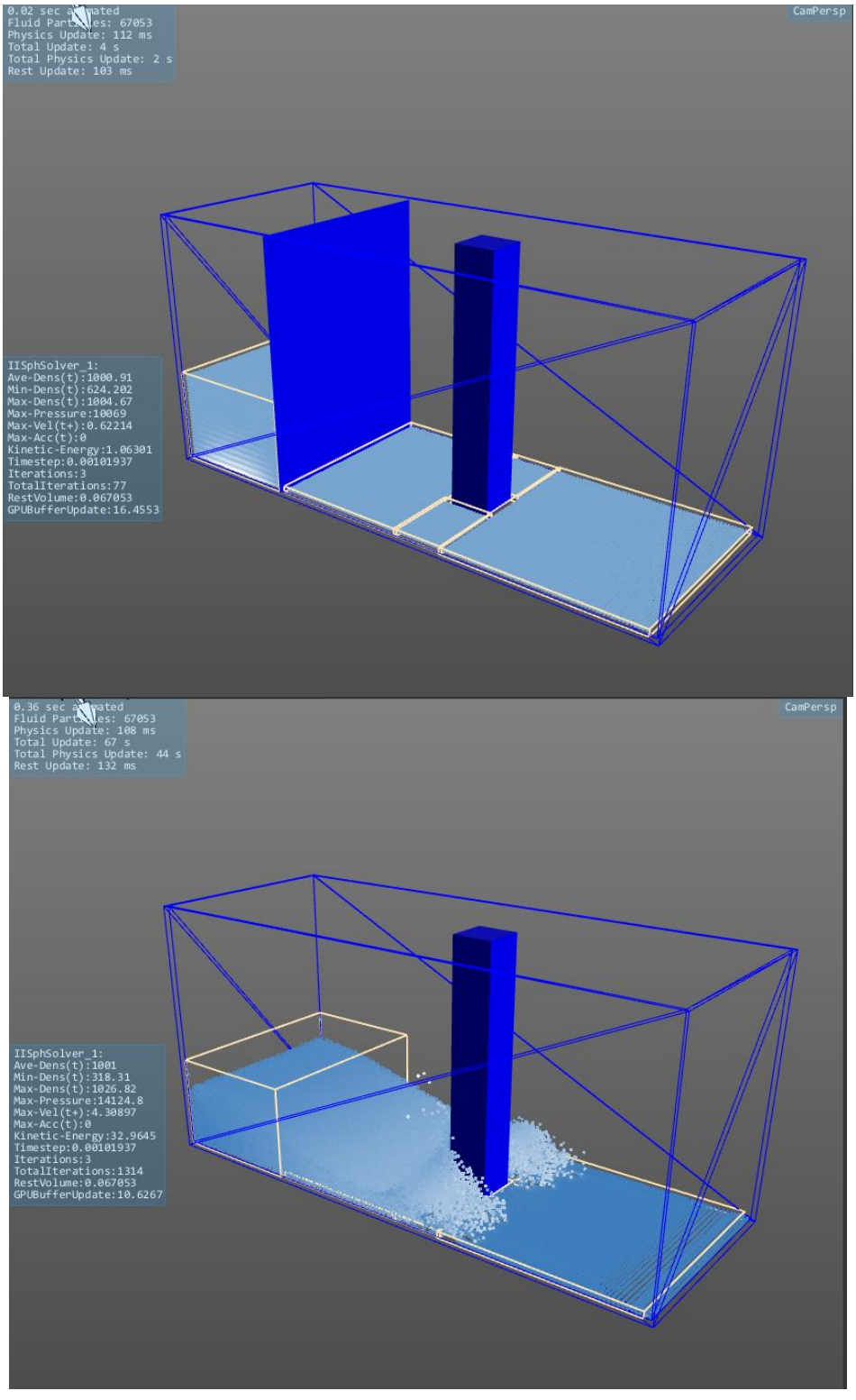
0.02 sec animated
Fluid Particles: 67053
Physics Update: 112 ms
Total Update: 4 s
Total Physics Update: 2 s
Rest Update: 103 ms
CamPersp
IISphSolver_1:
Ave-Dens(t):1000.91
Min-Dens(t):624.202
Max-Dens(t):1004.67
Max-Pressure:10069
Max-Vel(t+):0.62214
Max-Acc(t):0
Kinetic-Energy:1.06301
Timestep:0.00101937
Iterations:3
TotalIterations:77
RestVolume:0.067053
GPUBufferUpdate:16.4553
0.36 sec animated
Fluid Particles: 67053
Physics Update: 108 ms
Total Update: 67 s
Total Physics Update: 44 s
Rest Update: 132 ms
CamPersp
IISphSolver_1:
Ave-Dens(t):1001
Min-Dens(t):318.31
Max-Dens(t):1026.82
Max-Pressure:14124.8
Max-Vel(t+):4.30897
Max-Acc(t):0
Kinetic-Energy:32.9645
Timestep:0.00101937
Iterations:3
TotalIterations:1314
RestVolume:0.067053
GPUBufferUpdate:10.6267

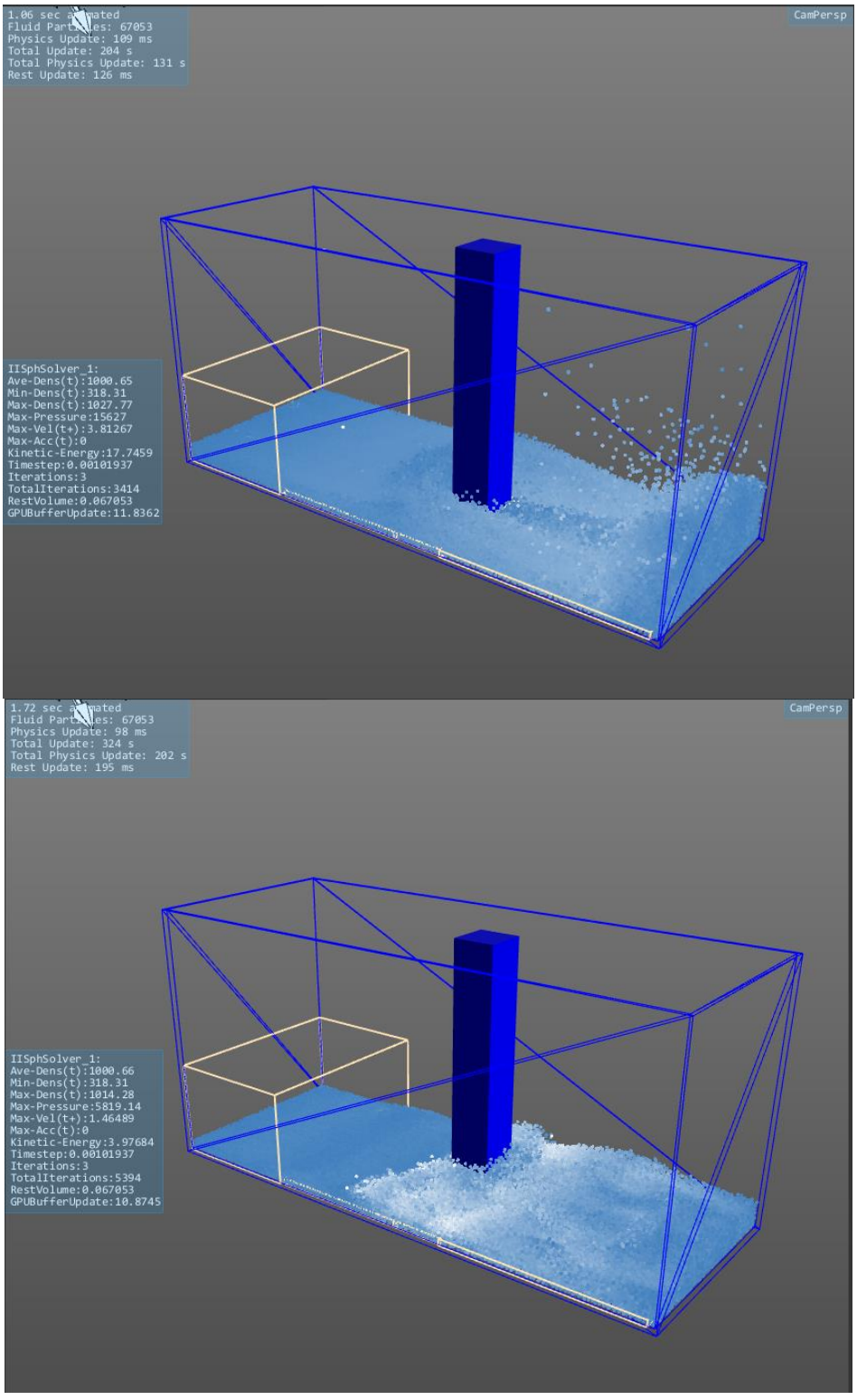

Figure 33: Evolution of the water collapse and interaction with the column simulated by Neutrino **[44]**.

Figure 34 shows comparison of measured forces from Neutrino outputs, with particle sizes equal to 0.1 and 0.01, to experimental data. It can be seen that more severe oscillation is obtained as the particle size is refined. This indicates that force of fluid-solid interaction may not converge and more works are needed for this measurement.

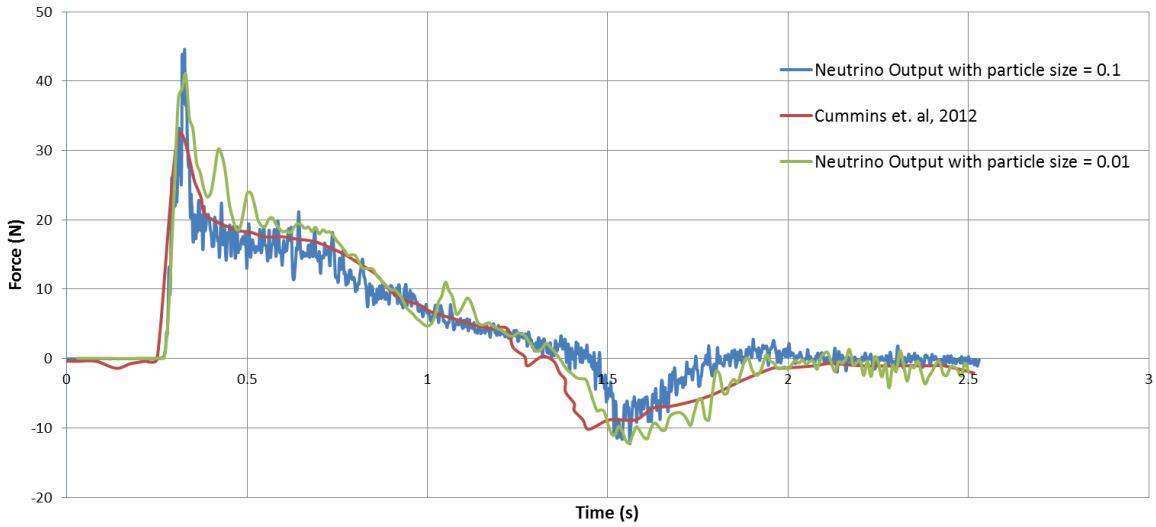

Figure 34: Comparison of Neutrino output with particle size = 0.1 and 0.01 to experimental data [50].

In general a pretty good agreement is found. Some discrepancy happens at the highest peak (around 0.3sec) and the lowest peak (around 1.5sec). The first peak, representing the first slamming from fluid to the dam structure, is higher than the experimental data because of the repulsive boundary treatment at fluid-solid interface. This repulsion can prevent penetration by exerting extra force to fluid particles, at the same time it exerts additional force to the rigid body.

3.3. Surface Tension Flow

3.3.1. Color, Normal, Curvature and Surface Tension Force Calculation

Based on the model of surface tension as from Eq. 15 - Eq. 19, the color, normal, curvature value and surface tension force are calculated. A spherical drop is put inside background fluid with the same density and viscosity. The contour plot of the transition region between the drop and background fluid is shown in Figure 35 on the left, also the surface tension force across the contour is shown on the right.

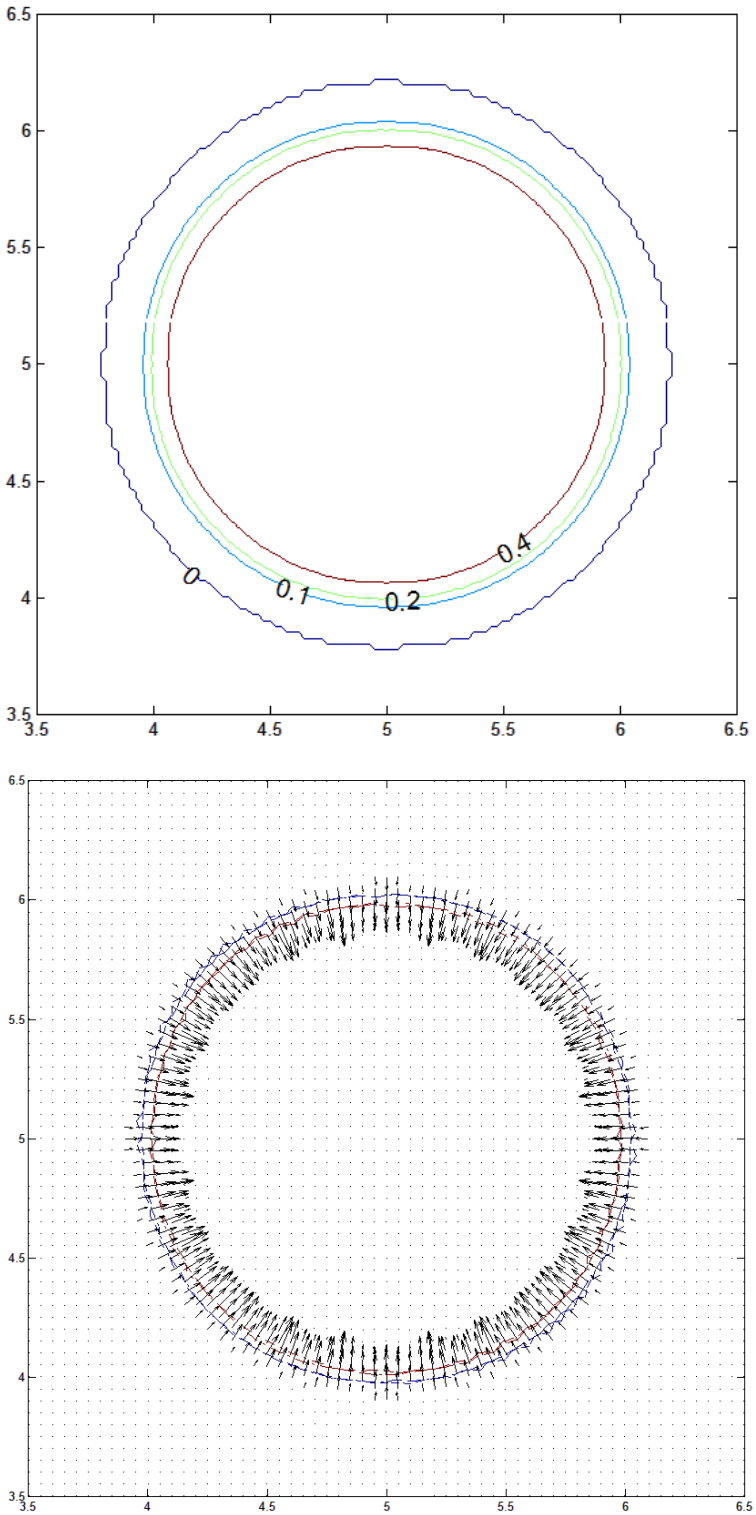

Figure 35: Contour plot (left) of color value for the transition between a drop and the background fluid and the surface tension force across the contour (right).

Besides, the color function, normal value, curvature and surface tension force across a square water bulk is measured and compared to Brackbill's [63] results as shown in Figure 36.. Because a finite thickness of fluid particles are applied to the interface, surface properties, including color function, normal value, curvature and surface tension force will be smoothed. This smoothing is believed to be necessary to ensure accuracy.

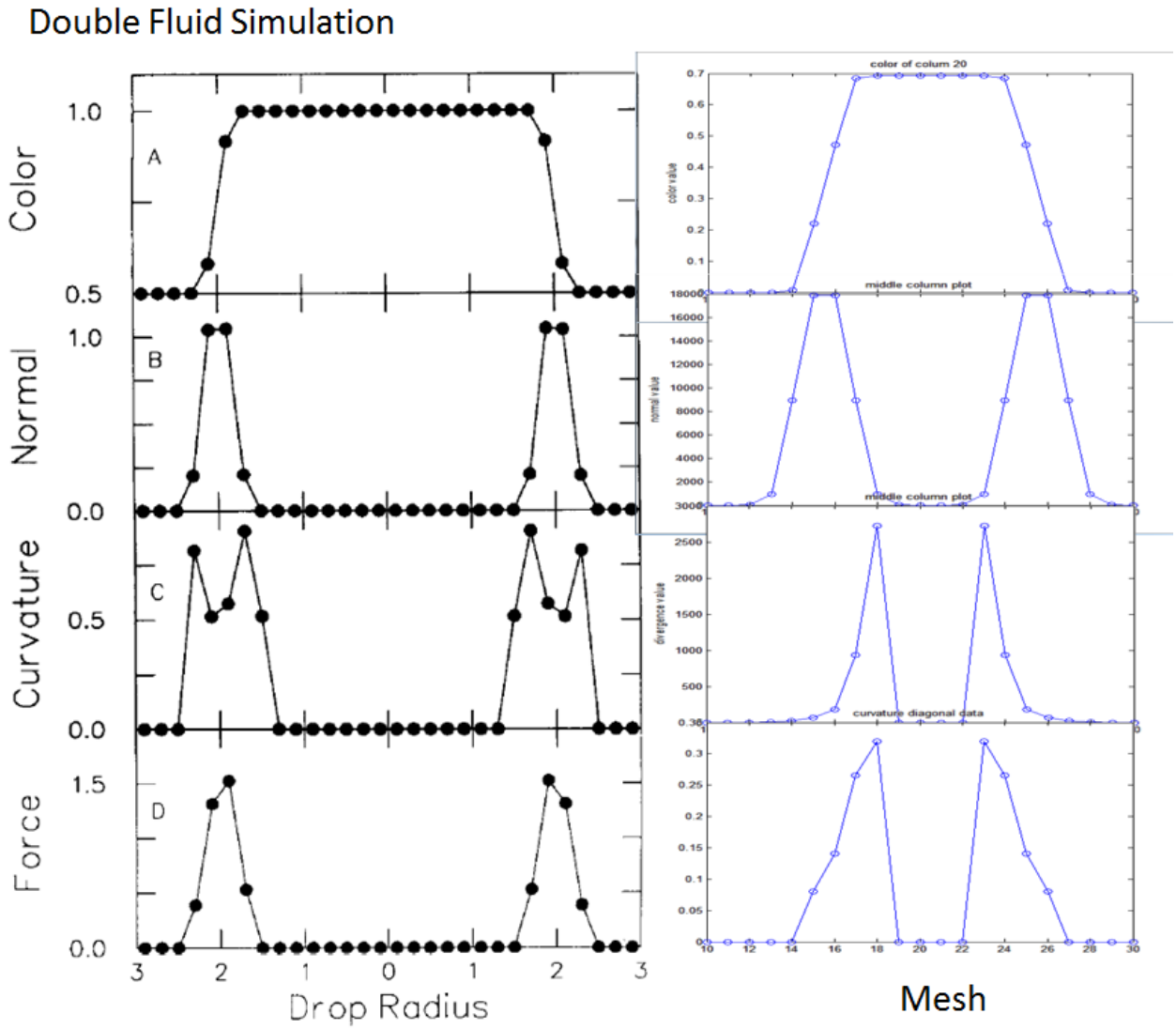

Figure 36: Plots of color function, magnitude of the normal vector, curvature and magnitude of surface tension force in a cut along the midline of the drop from Brackbill et al, 1992 **[63]** and our simulation.

3.3.2. Droplet Oscillation

In this simulation, a square water drop is put in vacuum with zero gravity. The drop will oscillate under the effect of surface tension and reach equilibrium state as a circle as shown in Figure 37. In viscous flow, the oscillation will only be damped by the numerical dissipation. We introduce viscosity in this case and assume there is no friction force on the interface. So the motion

will slow down and finally stabilize. The simulation results are shown in Figure 38. A good agreement is found between the theoretical and numerical solution.

Figure 37: Theoretical figure for the transition of square water drop into steady state as a circle

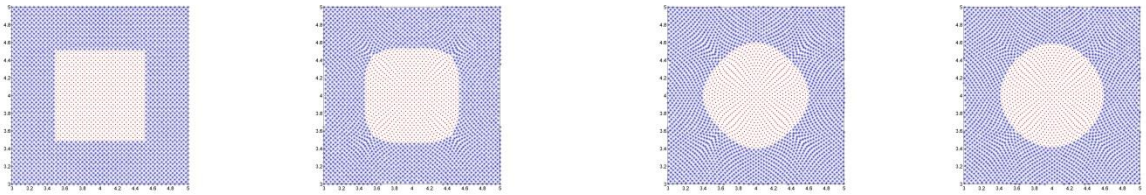

(a) (b) (c) (d)

Figure 38: Deform of initially square water bulk (marked as dot) at (a) 0.0, (b) 0.2, (c) 0.6 and (d) 1.4 in zero gravity and 0.1 viscosity. The initially square shape will deform under strong surface tension force at four corners, which have high curvature values. The surrounding fluid (marked as star) has the same viscosity and density.

The diameter is measured by searching for the SPH particle inside target fluid with largest horizontal distance and the one with smallest distance, then taking the difference and returning us the diameter of target fluid. Figure 39 shows the oscillation of droplet diameter with different particle size. And the oscillation will be damped by the viscosity to equilibrium state, the finally steady diameter is approximately 1.139. Also a clear converging progress can be seen as the particle size is reduced, which shows a good scalability of surface tension model in Micro-SPH.

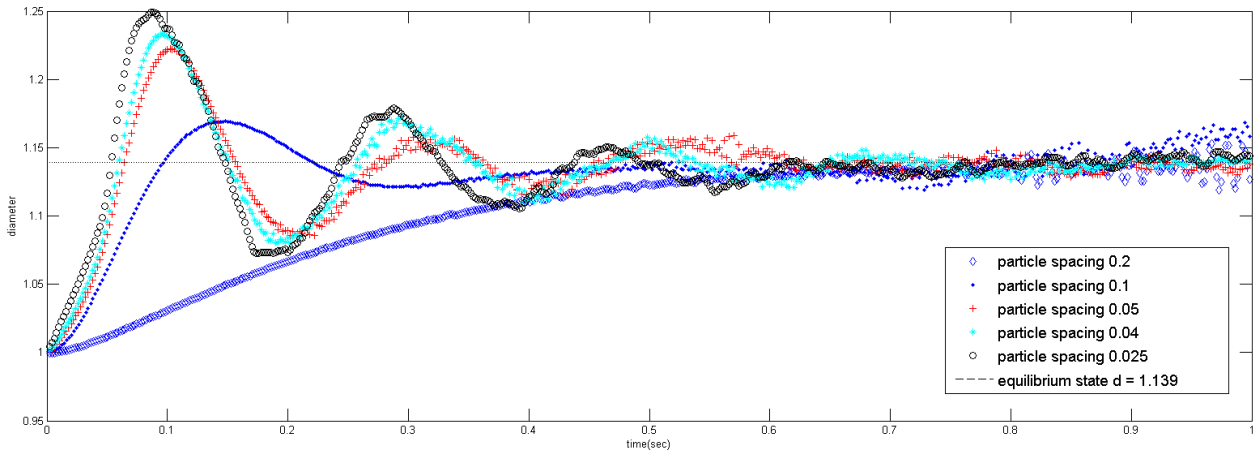

Figure 39: Oscillation of droplet diagram till equilibrium for different particle sizes.

Also the interface can be reconstructed by set up a user-defined color interval where the interface lays into, and particles are divided by the limit according to their color value. Figure 40 shows an example of interface reconstruction problem, in this case the color interval is set to be 0.3-0.5, which means all particles fall within the interval is selected to be interface particles. In order to make the interface continuous, the color interval may also change with the particle size.

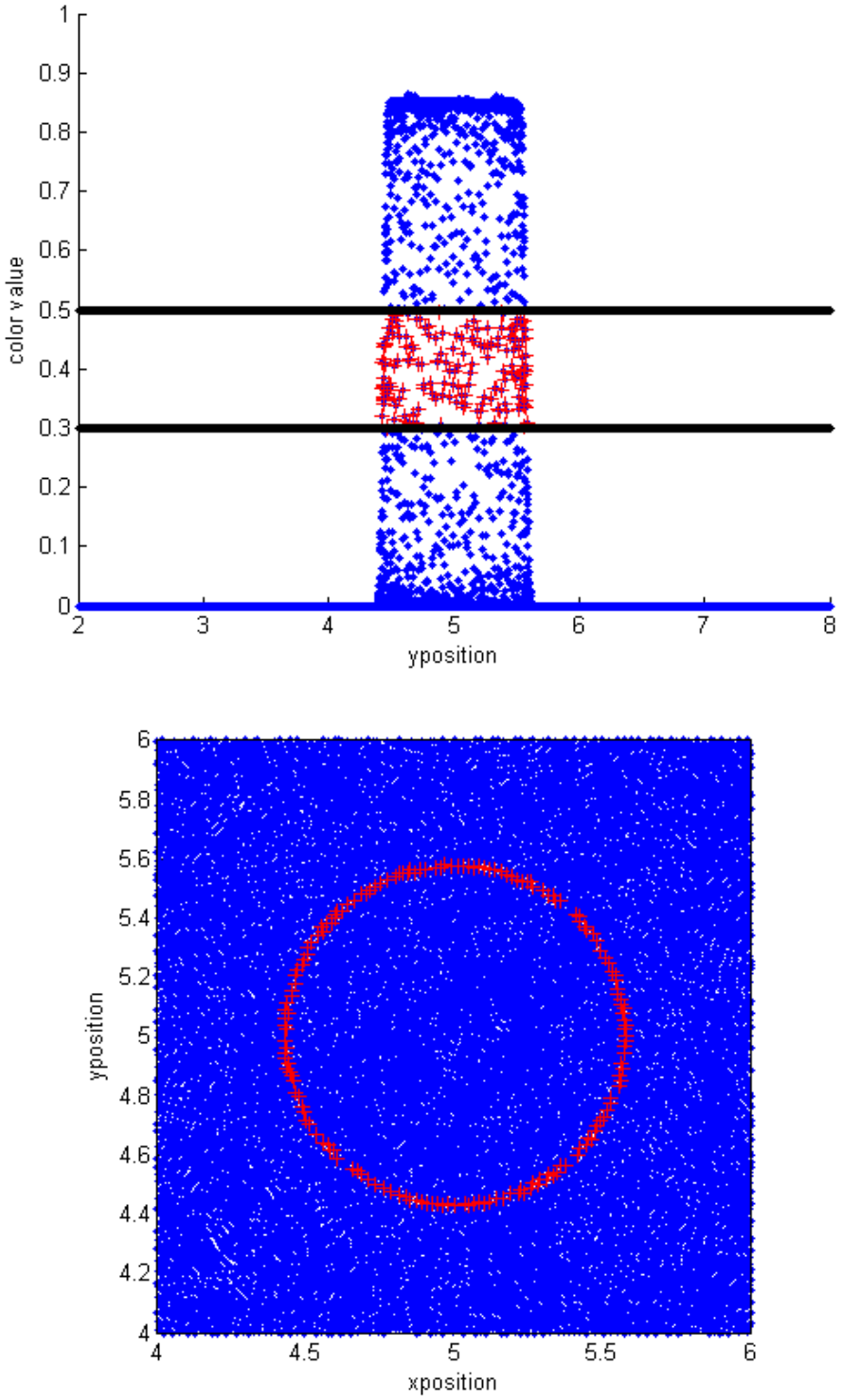

Figure 40: Interface reconstruction based on color value where color in range of 0.3~0.5 is set to be the limit to distinguish two fluid.

3.3.3. Surface Tension Effect

This simulation initially suspends a stable circle drop and makes it fall under the gravity onto the surface. By comparing the final states of fluid drops, the wetting capability of droplet is examined with different surface tension coefficient. It should be noted that the surface tension only acts on water droplet, the color, normal and divergence are always set to be zero for boundary particles. Or some unphysical phenomenon, like gap, will be visualized at the contact region between fluid and surface structure, which is very critical for this study. Figure 41 shows the shape of droplet with different surface tension coefficients.

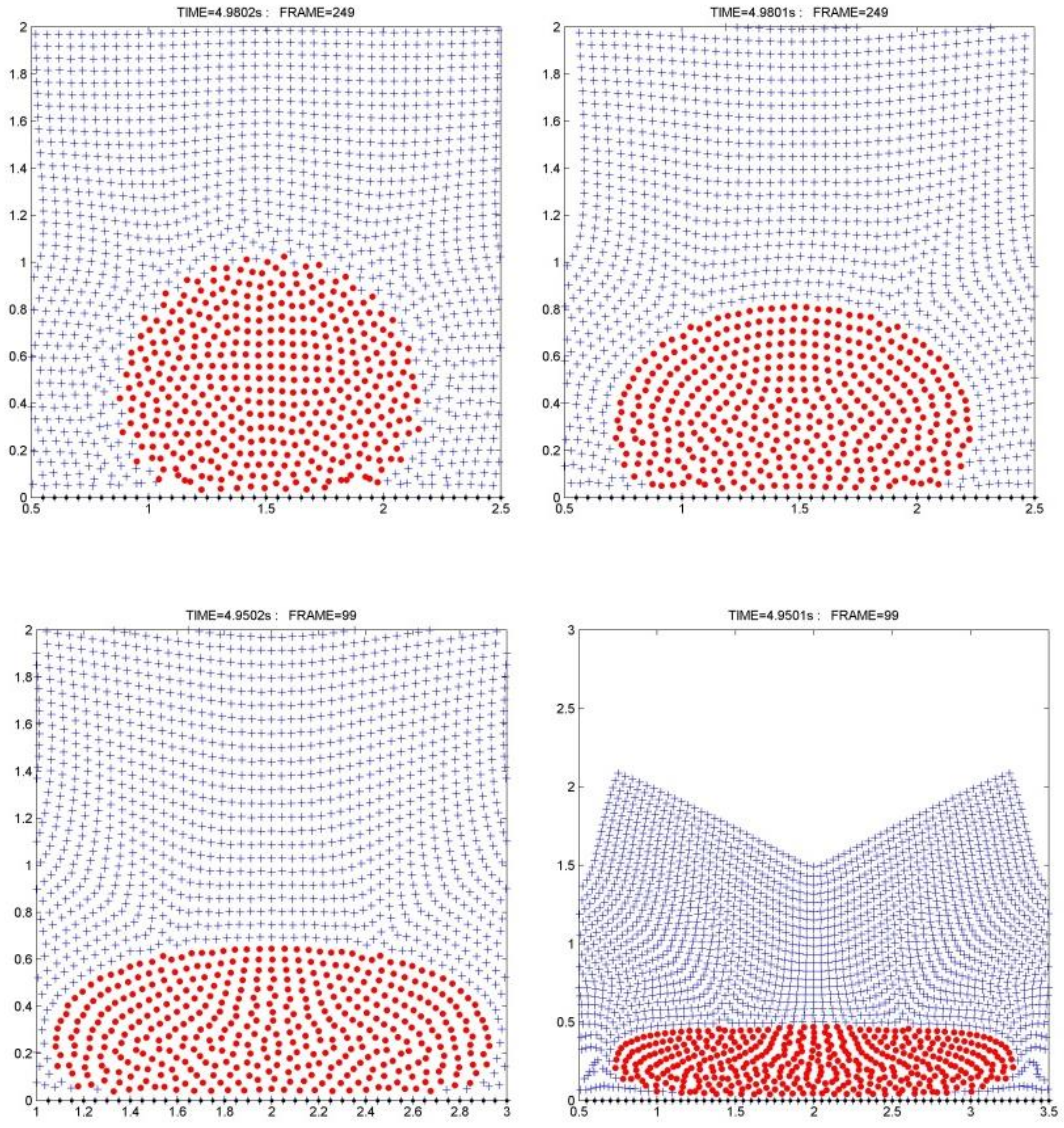

Figure 41: Final shape at 5sec of single drop under different surface tension coefficient (a) 5000 (Scale $\mathbf{2 \times 2}$), (b) 1000 (Scale $\mathbf{2 \times 2}$), (c) 500 (Scale $\mathbf{2 \times 2}$) and (d) 100 (Scale $\mathbf{3 \times 3}$) from left to right respectively.

In this case, gravity is the only factor that competes with the cohesion effects caused by surface tension force. So fluid with low surface tension has better wetting ability, and droplet tends to spread much wider than the one with 100 times higher surface tension. The contact angle for each surface tension setup is also measured and plotted again the gamma value.

3.4. Capillary Flow

3.4.1. Parallel Plates

In this simulation, an initially squared water drop is suspended between two parallel plates. Surface tension force is set to be zero so that only the effect of wettability is examined. Simulations are run for both wettability models. It turns out that model #2 tends to result in more penetration final shapes for each wettability coefficient are shown in

Figure 42. As the wettability coefficient β increasing, the edging particles climb higher. The radius of curvature of the receding interfaces is determined and listed in Table 6 and they are decreasing as the increasing of β.

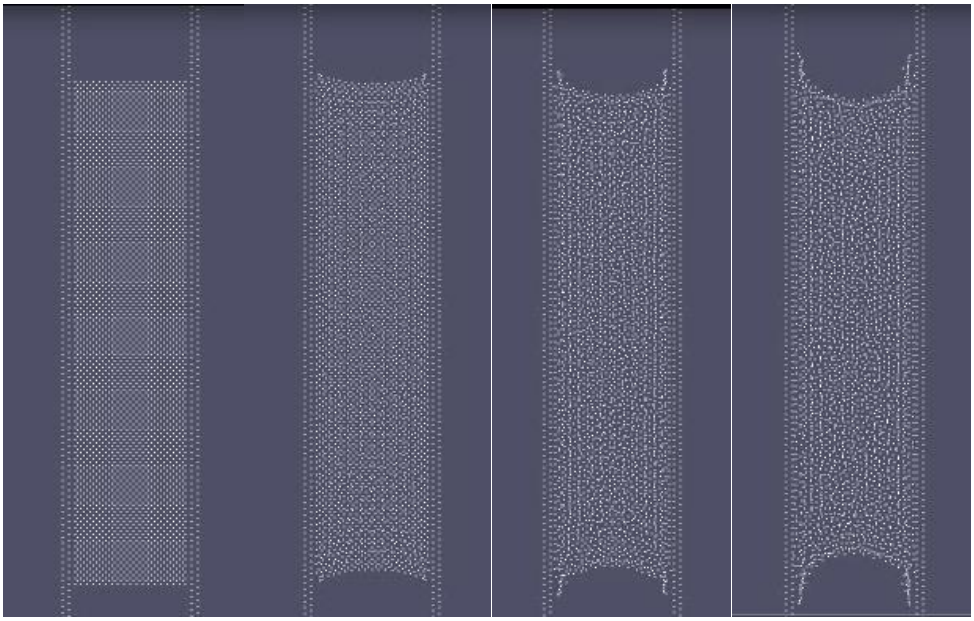

Figure 42: Final (5sec) shape of fluid between parallel plates with no surface tension and gravity, the wettability coefficient $\boldsymbol{\beta}$ is (a) 0, (b) 2, (c) 5 and (d) 10 from left to right respectively.

Table 6: Radii of receding interfaces for the stable fluid shape with different wettability coefficient $\boldsymbol{\beta}$ to be (a) 0, (b) 2, (c) 5 and (d) 10 from left to right respectively.

Stable state	Radius of receding interfaces
a	∞
b	1.3872
c	0.6647
d	0.4603

4. Discussion

Despite the above findings, two major issues should be noted about the current SPH methods. First, solution accuracy suffers severely in the area with low particle density. This might be caused by:

1. Particle size selection: Large particle size leads to information loss, while small particle size increases computational expenses. This is similar to the mesh size selection in the mesh-based methods.
2. Artificial term: Artificial term, especially the artificial compressibility, can lead to inaccuracy. As shown in Eq. 8, the pressure is function of a high power of the density. Figure 43 shows the plot of pressure against density ratio over reference density 1000kg/m^3. It can be seen that small disturbance in density can result in large and uneven fluctuations in. This problem will be shown in the simulation analysis below.

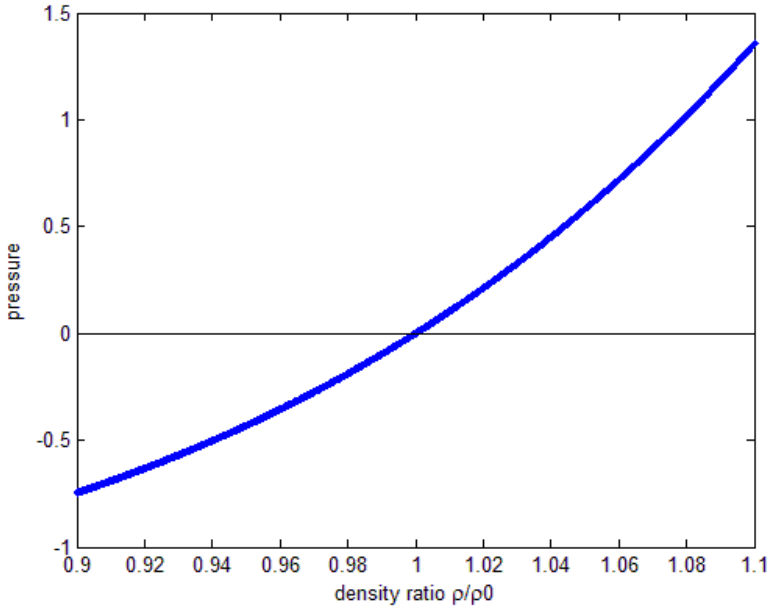

Figure 43: Pressure as function of density ratio calculated with Eq. 8.

The treatment of boundary is another major challenge for simulation accuracy. As mentioned in section 2.2.6, the compressibility is used to prevent particle penetration. On the other hand, it also attracts the particle away from the boundary, which could result in unphysical phenomenon (Figure 44). In addition, the placement of ghost particles is important, especially for curved or complex geometries, because SPH will search particles within its supporting domain.

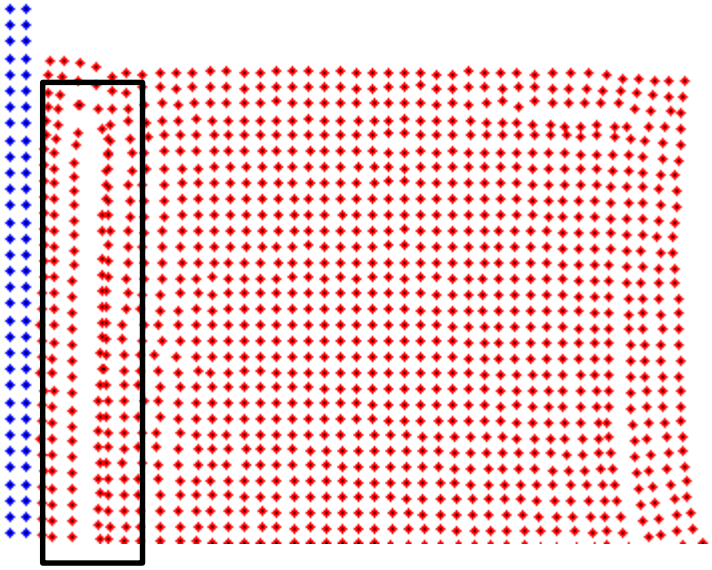

Figure 44: Particle vacancies due to high pressure gradient.

As for the efficiency, because adaptive particle size is hard to accomplish in SPH, very fine particle size may be needed for required accuracy. For simple problems, especially with single phase fluid, SPH is more computationally expensive than mesh-based methods. This is one of the major issues that limit the development of SPH in fluid dynamics in the past few decades. As the growth of computer power, and SPH suitability to parallel computing, this methods gain popularity, especially in computer graphic applications. In this study, the potential applicability of SPH to micro-scale simulations of interfacial phenomena suggest that this method might offer a more effective way to simulate boiling on textured surfaces compared to the traditional mesh-based methods.

For the boiling problem, modeling of heat transfer and phase change is still needed. Towards this end, the energy equation and a phase change model are required. In addition, the current wettability model is not capable of simulating very hydrophilic surfaces. Strong wettability coefficient will result in large pressure gradient and unphysical particle discontinuity. From the computational point of view, SPH needs adaptive particle size. Several algorithms developed [70] [71] are still limited in their ability to refine particles without strategy for particle aggregation.

5. Summary

This study assesses the capability of Smoothed Particle Hydrodynamics (SPH) in simulation of fluid at multiple scales. Multiple numerical experiments have been performed to evaluate the capability of SPH with respect to hydrodynamics, interface dynamics, and surface effects. Good agreement between SPH simulation results and fine-mesh CFD outputs or experimental results is observed in a number of cases.

A new program, Micro-SPH, based on SPHysics code is developed for micro-hydrodynamics applications. Two micro-hydrodynamic features (surface tension and wettability) are built into the mass and momentum equations.

Table 7 summarizes the findings and performance for the test cases.

Table 7: Summary of outcomes and findings for each test case and their degree of performance

Case Number	Findings	Degree of Performance
1. Poiseuille Flow	Layer(s) of stationary particles is capable of mimicking non-slip boundary Convergence rate is between 1st and 2nd order	Good
2. Collapse of Water Column	SPH can simulate free surface problems	Good
3. 3D Dam Break	SPH can produce reliable force/pressure estimate for fluid-solid interaction	Good
4. Flow Around Cylinder	SPH can capture flow pattern around and past cylinder obstacle with low Reynolds number	Good
	Pressure fluctuation happens near boundary. Weak vortex can be captured with high Reynolds number	To-be-addressed
5. Lid-Driven Cavity Flow	SPH can capture vortex with low Reynolds number	Good
	Unphysical vacancies appear with high Reynolds number	To-be-addressed
6. Color Function	SPH can track the interface between two phases	Good
7. Droplet Oscillation	SPH can simulate surface tension Surface tension model is convergent with particle size	Good
8. Drop Contacting Surface	SPH can simulate different wetting situations	Acceptable
9. Fluid between parallel plates	SPH can simulate capillarity and wettability phenomena	Acceptable

Based on the above findings, the SPH-based code is capable of simulating the effect of complex surface structures on the motion of thin liquid film .In addition, SPH method has capability for simulation of scenarios of flooding over complex terrain and facilities including

nuclear power plant. However, further development is needed to resolve the boundary treatment and efficiency issues.

REFERENCES

[1] T. N. Dinh and J. P. Tu, "The micro-hydrodynamics that govern critical heat flux in pool boiling," in *International Conference on Multiphase Flow*, Leipzig, 2007.

[2] T. G. Theofanous, T. N. Dinh, J. P. Tu and A. T. Dinh, "The boiling crisis phenomenon. Part II: critical heat flux and burn out," *Experimental Thermal FLuid Science,* vol. 26, no. 6-7, pp. 793-810, 2002.

[3] T. G. Theofanous, J. P. Tu, A. T. Dinh and T. N. Dinh, "The boiling crisis phenomenon. Part I: nucleation and nucleate boiling heat transfer," *Experimental Thermal and Fluid Science,* vol. 26, pp. 775-792, 2002.

[4] A. Betz, "Multiphase microfluidics for convective heat transfer and manufacturing," Columbia University, New York, 2011.

[5] B. J. Jones, J. B. McHale and S. V. Garimella, "The influence of surface roughness on nucleate pool boiling heat transfer," *Journal of Heat Transfer,* vol. 131, 2009.

[6] H. O'Hanley, C. Coyle, J. Buongiorno, T. McKrell and L. W. Hu, "Separate effects of surface roughness, wettability and porosity on the boiling critical heat flux," *Applied Physics Letters,* vol. 103, 2013.

[7] K. H. Chu, R. Enright and E. Wang, "Structured surfaces for enhanced pool boiling heat transfer," *Applied Physics Letters,* vol. 100, 2012.

[8] O. A. Kabov, D. V. Zaitsev, V. V. Cheverda and A. Bar-Cohen, "Evaporation and flow dynamics of think, shear-driven liquid films in microgap channels," *Experimental Thermal dna FLuid Science,* vol. 35, pp. 825-831, 2011.

[9] K. J. Geisler and A. B. Cohen, "Confinement effects on nucleate boiling and critical heat flux in buoyancey-driven microchannels," *International Journal of Heat and Mass Transfer,* vol. 52, pp. 2427-2436, 2009.

[10] S. G. Kandlikar, "A theoretical model to predict pool boiling CHF incorporating effects of contact angle and orientation," *Journal of Heat Transfer,* vol. 23, pp. 1071-1079, 2011.

[11] S. W. Ahmad, T. G. Karayiannis, D. Kenning and A. Luck, "Compount effect of EHD and surface roughness in pool boiling and CHF with R-123," *Applied Thermal Engineering* , vol. 31, no. 11-12, pp. 1994-203, 2011.

[12] Y. Sato and B. Niceno, "A depletable micro-layer model for nucleate pool boiling," *Journal of Computational Physics,* vol. 300, pp. 20-52, 2015.

[13] D. Kim, D. Yu, S. Park, H. Kwak and H. Ahn, "Critical heat flux triggering mechanism on micro-structure surfaces: coalesced bubble departure frequency and liquid furnishing capability," *International Journal of Heat and Mass Transfer,* vol. 91, pp. 1237-1247, 2015.

[14] A. Oron, S. Davis and S. Bankoff, "Long-scale evolution of thin liquid films," *Reviews of Modern Physics,* vol. 69, pp. 931-980, 1997.

[15] M. Ishii and K. Mishima, "Two-fluid model and hydrodynamic constitutive relations," *Nuclear Engineering and Design,* vol. 82, no. 2-3, pp. 107-126, 1984.

[16] H. Stadtke, Gasdynamic aspects of two-phase flow: hyperbolicity, wave propagation phenomena, and related numerical methods, Weinheim: WILEY-VCH Verlag GmbH & Co. KGaA, 2007.

[17] M. Ishii and N. Zuber, "Drag coefficient and relative velocity in bubbly, droplet or particulate flows," *AIChE J,* vol. 25, p. 843, 1979.

[18] N. Zuber, "On the despersed two-phase flow on the laminar flow regime," *Chemical Engineering and Science,* vol. 19, p. 897, 1964.

[19] M. Ishii and K. Mishima, "Study of two-fluid model and interfacial area," Argonne National Laboratory, 1981, 1981.

[20] S. Osher and J. Sethian, "Fronts propagating with curvature-dependent speed: algorithms based on Hamilton-Jacobi formulations," *Journal of Computational Physics,* vol. 79, no. 1, pp. 12-49, 1988.

[21] M. Sussman, P. Smereka and S. Osher, "A level set approach for computing solutions to incompressible two-phase flows," *Journal of COmputational Physics,* vol. 114, pp. 146-159, 1994.

[22] W. Noh and P. Woodward, "SLIC (simple line interface calculation)," in *Fifth International Conference on Fluid Dynamics,* Berlin, 1976.

[23] C. Hirt and B. Nichols, "Volume of fluid (VOF) method for the dynamics of free boundaries," *Journal of Computational Physics,* vol. 39, pp. 201-226, 1981.

[24] M. Gomez-Gesteira, B. D. Rogers, A. J. Crespo, R. A. Dalrymple, M. Narayanaswamy and J. M. Dominguez, "SPHysics-development of a free-surface fluid solver- part 1: theory and formulations," 2012. [Online]. Available: http://www.sphysics.org. [Accessed 25 Feburary 2016].

[25] "LAMMPS-SPH," [Online]. Available: http://lammps.sandia.gov.

[26] J. J. Monaghan, "Simulating free surface flow with SPH," *Journal of COmputational Physics,* vol. 110, pp. 399-406, 1994.

[27] M. B. Liu and G. R. Liu, "Smoothed Particle Hydrodynamics (SPH): an overview and recent developments," *Archives of Computational Methods in Engineering,* vol. 17, pp. 25-76, 2010.

[28] M. Steinmetz and E. Muller, "On the capabilities and limits of smoothed particle hydrodynamics," *Astronomy and Astrophysics,* vol. 268, no. 1, pp. 391-410, 1992.

[29] W. Benz, "Smoothed Particle Hydrodynamics: a review," *The Numerical Modelling of Nonlinear Stellar Pulsations,* vol. 302, pp. 269-288, 1990.

[30] H. Kao and T. Chang, "Numerical modeling of dambreak0induced flood and inundation using smoothed particle hydrodynamics," *Journal of Hydrology,* Vols. 448-449, pp. 232-244, 2012.

[31] R. A. D. M.G. Gesteira, "Using a three-dimensional smoothed particle hydrodynamics method for wave impact on a tall structure," *Journal of Waterway, Port, Coastal, and Ocean Engineering,* vol. 130, no. 2, 2004.

[32] G. R. Liu and M. B. Liu, Smoothed Particle Hydrodynamics, a meshfree particle method, World Scientific, 2013.

[33] R. Sharp, "The nature of liquid film evaporation during nucleat boiling," in *NASA TN D-1997*, 1964.

[34] H. Jawurek, "Simultaneous determination of microlayer geometry and bubble growth in nucleat boiling," *International Journal of Heat and Mass Transfer,* vol. 12, pp. 843-848, 1969.

[35] T. yabuki and O. Nakabeppu, "Heat transfer mechanisms in isolated bubble boiling of water observed with MEMS sensor," *International Journal of Heat and Mass Transfer*, vol. 12, pp. 895-913, 1969.

[36] V. Team, "How to PIRT," Sandia National Laboratories, Albuquerque.

[37] N. Paragios and R. Deriche, "Geodesic active regions and level set methods for supervised texture segmentation," *International Journal of Computer Vision*, vol. 46, no. 3, pp. 223-247, 2002.

[38] J. Sethian and P. Smereka, "Level set methods for fluid interfaces," *Annual Review of Fluid Mechanics*, vol. 35, pp. 341-372, 2003.

[39] P. J. Hoogerbrugge and J. Keolman, "Simulating microscopic hydrodynamic phenomena with dissipative particle dynamics," *Europhysics Letters*, vol. 19, no. 3, pp. 155-160, 1992.

[40] R. A. Gingold and J. J. Monaghan, "Smoothed Particle Hydrodynamics: theory and application to non-spherical star," *Monthly Notices of the Royal Astronomical Society*, pp. 375-389, 1977.

[41] R. G. Sargent, "Verification and validation of simulation models," in *Proceedings of the 2005 Winter Simulation Conference*, 2005.

[42] Schlesinger, "Terminology for model credibility," *Simulation*, vol. 32, no. 3, pp. 103-104, 1979.

[43] "Transient and accident analysis methods regulatory guide report No. 1.203," U.S. Nuclear Regulatory Commission, Washington D.C., 2002.

[44] "NEUTRINO," [Online]. Available: http://www.neutrinodynamics.com.

[45] N. Akinci, "Interface handling in smoothed particle hydrodynamics," Albert-Ludwigs-Universität, Freiburg, 2014.

[46] N. Akinci, G. Akinci and M. Teschner, "Versatile surface tension and adhesion for SPH," in *ACM Transaction on Graphics*, 2013.

[47] N. Akinci, M. Ihmsen, G. Akinci, B. Solenthaler and M. Teschner, "Versatile rigid-fluid coupling for incompressible SPH," in *ACM Transaction on Graphics*, 2012.

[48] M. Ihmasen, J. Cornelis, B. Solenthaler, C. Horvath and M. Teschner, "Implicit Incompressible SPH," *IEEE Transactions on Visualization and Computer Graphics,* vol. 20, 2014.

[49] "SMD_LAMMPS," [Online]. Available: https://github.com/jluissandovalm/smd_lammps.

[50] "LAMMPS-SPH-multiphase," [Online]. Available: https://github.com/slitvinov/lammps-sph-multiphase.

[51] L. B. Lucy, "A numerical approach to the testing of the fission hypothesis," *Astronomical Journal,* vol. 82, no. 12, pp. 375-389, 1977.

[52] R. A. Gingold and J. J. Monaghan, "Kernel estimates as a basis for general particle method in hydrodynamics," *Journal of Computational Physics,* vol. 46, pp. 429-453, 1982.

[53] X. Y. Hu and N. A. Adams, "Angular-momentum conservative smoothed particle dynamics for incompressible viscous flow," *Physics of Fluids,* vol. 18, 2006.

[54] J. J. Monaghan, "Smoothed Particle Hydrodynamics," *Annual Revision Astronomy Application,* vol. 30, pp. 543-574, 1992.

[55] G. R. Liu, Mesh free methods: moving beyond the finite element method, New York: CRC Press, 2003.

[56] H. Wendland, "Piecewise polynomial, positive definite and compactly supported radial functions of minimal degree," *Advances in Computational Mathematics,* vol. 4, no. 1, pp. 398-396, 1995.

[57] J. P. Morris, P. J. Fow and Y. Zhu, "Modeling low Reynolds number incompressible flows using SPH," *Journal of Computational Physics,* vol. 136, pp. 214-226, 1997.

[58] J. P. Morris, "Simulating surface tension with smoothed particle hydrodynamics," *International Journal of Numerical Methods in Fluids,* vol. 33, pp. 333-353, 2000.

[59] L. M. Gonzalez, J. M. Sanchez, F. Macia and A. Souto-Iglesia, "Analysis of WCSPH laminar viscosity model," in *4th international SPHERIC workshop,* Nantes, 2009.

[60] F. A. Allahdadi, T. C. Carney, F. R. Hipp and L. D. Libersky, "High strain Lagrangian hydrodynamics-a three-dimensional SPH code for dynamics material response," in *Proceeding of the Next Free Lagrange COnference,* New York, 1991.

[61] G. R. Liu and Y. T. Gu, "A local radial point interpolation method (LR-PIM) for free vibration analyses of 2D solids," *Journal of Sound and Vibration,* vol. 246, no. 1, pp. 29-46, 2001.

[62] A. Leroy, "A new incompressible SPH model: towards industrial applications, Modeling and Simulation," University Paris-Est, 2014.

[63] J. U. Brackbill, D. B. Kothe and C. Zemach, "A continuum method for modeling surface tension," *Journal of Computational Physics,* vol. 100, pp. 335-354, 1992.

[64] A. Tartakovsky and P. Meakin, "Modeling of surface tension and contact angles with smoothed particle hydrodynamics," *Physical Review,* vol. 72, 2005.

[65] S. Shahriari and I. K. L. Hassan, "Modeling unsteady flow characteristics using smoothed particle hydrodynamics," *Applied Mathematical Modeling,* vol. 37, pp. 1431-1450, 2013.

[66] R. Fatehi and M. T. Manzari, "Error estimation in smoothed particle hydrodynamics and a new scheme for second derivatives," *computers & Mathematics with Applications,* vol. 61, pp. 482-498, 2011.

[67] S. Koshizuka, H. Tamako and Y. Oka, "A particle method for incompressible viscous flow with fluid gragmentation," *Computational Fluid Dynamics Journal,* vol. 4, p. 29, 1995.

[68] J. C. Martin and W. J. Moyce, "An experimental study of the collapse of liquid columns on a rigid horizontal plan," *Philosophical Transactions of the Royal Society A,* vol. 244, p. 312, 1952.

[69] S. J. Cummins, T. B. Silverster and P. W. Cleary, "Three-dimensional wave impact on a rigid structure using smoothed particle hydrodynamics," *International Journal for Numerical Methods in Fluids,* vol. 68, pp. 1471-1496, 2012.

[70] R. Vacondio, B. D. Rogers, P. K. Stansby and P. Mignosa, "SPHysics," March 2013. [Online]. Available: https://wiki.manchester.ac.uk/sphysics/images/SWE-SPHysics_v1.0.00.pdf. [Accessed 25 Feburary 2016].

[71] S. Barbara and G. Markus, "Two-scale particle simulation," *ACM Transactions on Graphics - Procedings of ACM SIGGRAPH 2011,* vol. 30, no. 4, 2011.

[72] R. H. Perkins, M. T. Bensi, J. Philip and S. Sancaktar, "Screening analysis report for the proposed generic issue on flooding of nuclear power plant sites following upstream dam failures," U.S. Nuclear Regulatory Commission, Washington D.C., 2011.

[73] D. L. Huang and S. H. Abdel-Khalik, "Mapping of biases and uncertainties from fresh fuel experiments to depleted fuel," 2015.

[74] S. H. Adel-Khalik, H. I. Ayman and C. Wang, "Physics-guided covered mapping: a new approach for quantifying experimental coverage and bias scaling," *Transcations of the American Nuclear Society,* vol. 112, pp. 704-707, 2015.

[75] E. Parish and K. Duraisamy, "A paradigm for data-driven predictive modeling using field inversion and machine learning," *Journal of Computational Physics,* vol. 305, pp. 759-774, 2016.

[76] R. King and P. Hamlington, "Autonomic subgrid-scale closure for large eddy simulations," in *53rd AIAA Aerospace Sciences Meeting*, Florida, 2015.

[77] R. King, P. Hamlington and W. Dahm, "A new autonomic closure for large eddy simulations," in *International Symposium on Turbulence and Shear Flow Phenomena*, Melbourne, 2015.

APPENDICES

Appendix A
List of Micro-SPH subroutines

Functions in bold are designed specifically for Micro-SPH, while others are inherited from SPHysics

ac_2D.f	Main function for calculating the particle acceleration due to viscosity
adhesion_kernel.f	Fourth order kernel function for adhesion calculation, called from cohesion cell and self every time
celij_BC_Dalrymple_2D.f	Calculate interaction due to viscosity between particles inside adjacent cells from the link list
coh_cal_celij.f	Calculate interaction due to cohesion/adhesion force between particles inside adjacent cells from the link list, called from cohesion_function.f
coh_cal_selfij.f	Calculate interaction due to cohesion/adhesion force between particles inside the same cells from the link list, called from cohesion_function.f
cohesion_function.f	Main function for calculating the particle acceleration due to adhesion/cohesion
color_cal_celij.f	Calculate color value for particles inside adjacent cells from the link list, called from color_function.f
color_cal_selfij.f	Calculate color value for particles inside the same cells from the link list, called from color_function.f
color_function.f	Main function for calculating the color value
color_index.f	Designate area for different types of particles, used for multi-fluid calculation
correct_2D.f	Calculate acceleration due to body force
divide_2D.f	Called every time step, and creates link list
div_cal_celij.f	Calculate divergent value for particles inside adjacent cells from the link list, called from div_function.f
div_cal_selfij.f	Calculate divergent value for particles inside the same cells from the link list, called from div_function.f
div_function.f	Main function for calculating the divergent value
EoS_Tait_2D.f	Calculate the pressure using Eq. 8
fcurv_function.f	Main function for calculating the surface tension force
getdata_2D.f	Called at the beginning of run, get data from input file
keep_list.f	Keep the list of fixed boundary particles
kernel_cubic_2D.f	Cubic kernel function, called for every self and cell calculation except for cohesion/adhesion
kernel_wendland5_2D.f	Fifth order kernel function, called for every self and cell calculation except for cohesion/adhesion

norm_cal_celij.f	Calculate (unit)norm value for particles inside adjacent cells from the link list, called from norm_function.f
norm_cal_selfij.f	Calculate (unit)norm value for particles inside the same cells from the link list, called from norm_function.f
norm_function.f	Main function for calculating the norm value
poute_2D.f	Output data
self_BC_Dalrymple.f	Calculate interaction due to viscosity between particles inside the same cells from the link list
step_predictor_corrector_2D.f	Called every time step, calculate the particle acceleration and determine particle moving
SPHYSICS_2D.f	main time loop
viscosity_artificial_2D.f	Calculate viscosity with artificial viscosity formula Eq. 11
viscosity_laminar_2D.f	Calculate viscosity with laminar viscosity formula Eq. 13

Appendix B
Code structure of subroutines listed in Appendix A